

AFOSR-TR-85-0288

2

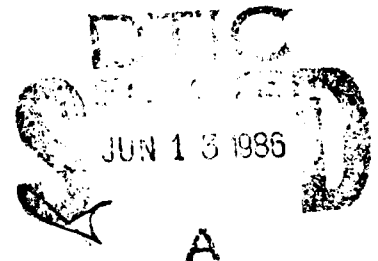
AD-A168 491

INVESTIGATION OF AN ASYMPTOTIC EXPANSION  
TECHNIQUE TO ANALYZE LIMIT CYCLE  
RESPONSE OF AERODYNAMIC SURFACES  
WITH STRUCTURAL NONLINEARITIES

Anthony J. Hauenstein  
Robert M. Laurenson  
John L. Gubser

8 July 1985

This work was sponsored by  
The Air Force Office of Scientific Research  
Under Contract Number: F49620-84-C-0123



**MCDONNELL DOUGLAS ASTRONAUTICS COMPANY**  
**ST. LOUIS DIVISION**  
Box 516, Saint Louis, Missouri 63166

**MCDONNELL DOUGLAS**  
CORPORATION

86 6 10 126

UNCLASSIFIED

SECURITY CLASSIFICATION OF THIS PAGE (When Data Entered)

REPORT DOCUMENTATION PAGE		READ INSTRUCTIONS BEFORE COMPLETING FORM
1. REPORT NUMBER	2. GOVT ACCESSION NO.	3. RECIPIENT'S CATALOG NUMBER
AFOSR TR- 88-0288		ADA163491
4. TITLE (and Subtitle)		5. TYPE OF REPORT & PERIOD COVERED
INVESTIGATION OF AN ASYMPTOTIC EXPANSION TECHNIQUE TO ANALYZE LIMIT CYCLE RESPONSE OF AERODYNAMIC SURFACES WITH STRUCTURAL NONLINEARITIES		Final Report 13 Sep 84 - 13 Jul 85
7. AUTHOR(s)		6. PERFORMING ORG. REPORT NUMBER
Anthony J. Hauenstein Robert M. Laurenson John L. Gubser		
9. PERFORMING ORGANIZATION NAME AND ADDRESS		8. CONTRACT OR GRANT NUMBER(s)
McDonnell Douglas Astronautics - St. Louis Div. P.O. Box 516 St. Louis, MO 63166		F49620-84-C-0123
11. CONTROLLING OFFICE NAME AND ADDRESS		10. PROGRAM ELEMENT, PROJECT, TASK AREA & WORK UNIT NUMBERS
Air Force Office of Scientific Research / 2A Bolling Air Force Base Washington, DC 20332		61102F 2307/B1
14. MONITORING AGENCY NAME & ADDRESS (if different from Controlling Office)		12. REPORT DATE
		8 July 1985
		13. NUMBER OF PAGES
		49
		15. SECURITY CLASS. (of this report)
		Unclassified
		15a. DECLASSIFICATION/DOWNGRADING SCHEDULE
16. DISTRIBUTION STATEMENT (of this Report)		
Approved for public release; distribution unlimited.		
17. DISTRIBUTION STATEMENT (of the abstract entered in Block 20, if different from Report)		
18. SUPPLEMENTARY NOTES		
19. KEY WORDS (Continue on reverse side if necessary and identify by block number)		
Limit Cycle Oscillation Structural Nonlinearity Flutter Analysis		
20. ABSTRACT (Continue on reverse side if necessary and identify by block number)		
Defining the flutter and divergence characteristics of aerodynamic surfaces is a basic requirement in assuring structural and performance integrity of a given design for its operational environment. Divergence and flutter phenomena are unstable motions with increasing amplitude. For systems containing structural nonlinearities, another mode of aeroelastic response--limit cycle oscillation--may be present. The potential of limit cycle response is of importance since these oscillations may occur within the aerodynamic surface		

UNCLASSIFIED

SECURITY CLASSIFICATION OF THIS PAGE(When Data Entered)

20. ABSTRACT (Continued)

flutter and divergence flight envelope and may lead to fatigue damage of the system even though aeroelastic instability is not encountered.

During a previous AFOSR sponsored study, an asymptotic expansion approximation technique was developed to predict the limit cycle response of aerodynamic surfaces with discrete structural nonlinearities. As a part of this study, numerical simulation results were used to evaluate the adequacy of the asymptotic expansion solutions to the nonlinear problem. A "simple" trapezoidal numerical integration procedure was used to obtain these simulation results. Results of this previous study uncovered shortcomings with the trapezoidal integration scheme. Based on these results it was concluded that the application of more refined integration techniques to the nonlinear aerodynamic surface problem needed to be investigated.

Thus the present study was undertaken with the objective to evaluate, on a comparative basis, different numerical simulation approaches for predicting limit cycle response of aerodynamic surfaces containing discrete structural nonlinearities. Results from such simulations are needed to compare and evaluate approximate solutions for the limit cycle response of nonlinear systems. In addition, these simulation results provide information concerning the nature of the nonlinear system response which may be used to aid in understanding the mechanism of the aerodynamic surface dynamics and in understanding the response of nonlinear systems in general.

Three numerical integration techniques were selected for evaluation: (1) fourth-order Runge-Kutta, (2) eighth-order Shanks, and (3) fourth-order Adams-Moulton predictor-corrector. The results of the three simulation techniques compared well with each other. In addition they yielded improved correlation with previously developed approximate solutions when compared to the correlation of the approximate solutions using the trapezoidal integration scheme. It was concluded that any one of the three numerical techniques is appropriate for use in determining limit cycle response of an aerodynamic surface containing discrete structural nonlinearities. From a computational efficiency point of view, the Runge-Kutta approach appears most attractive for this type of problem.

In spite of the improved results obtained with the numerical integration techniques evaluated during this study, there remain regions where the correlation between numerical and approximate prediction is inconsistent. The need for additional research to address these inconsistencies has been identified. This research will provide an improved understanding of the nonlinear response characteristics of an aerodynamic surface containing discrete structural nonlinearities.



Acquisition Code

17

UNCLASSIFIED

SECURITY CLASSIFICATION OF THIS PAGE(When Data Entered)

## ACKNOWLEDGMENT

This report was prepared by the Structural Dynamics and Loads Department, McDonnell Douglas Astronautics Company-St. Louis, Missouri, under Contract F49620-84-C-0123, "Investigation of an Asymptotic Expansion Technique to Analyze Limit Cycle Response of Aerodynamic Surfaces with Structural Non-linearities." The program was administered under the direction of the Air Force Office of Scientific Research with Dr. Anthony K. Amos as Program Manager.

AIR FORCE OFFICE OF SCIENTIFIC RESEARCH (AFOSR)  
DISTRIBUTION STATEMENT UNCLASSIFIED  
REPORT NUMBER AFOSR-84-0123  
AFOSR-84-0123-12  
MATTIE  
Chief, Technical Information Division

## TABLE OF CONTENTS

	<u>Page</u>
1.0 INTRODUCTION.....	1
2.0 NUMERICAL INTEGRATION TECHNIQUES.....	10
2.1 FOURTH-ORDER RUNGE-KUTTA.....	12
2.2 EIGHTH-ORDER SHANKS.....	13
2.3 FOURTH-ORDER ADAMS-MOULTON.....	15
3.0 NUMERICAL SIMULATION RESULTS.....	17
3.1 RIGID AERODYNAMIC SURFACE.....	17
3.2 FLEXIBLE AERODYNAMIC SURFACE.....	20
4.0 CONCLUSIONS.....	31
5.0 REFERENCES.....	35
APPENDICES	
A. AERODYNAMIC SURFACE CONFIGURATION.....	37
B. SIMULATION RESULTS FOR FLEXIBLE AERODYNAMIC SURFACE.....	41

## LIST OF ILLUSTRATIONS

<u>Figure</u>	<u>Title</u>	<u>Page</u>
1	Models of Aerodynamic Surface Aeroelastic Response.....	2
2	Type of Structural Nonlinearities.....	3
3	Aerodynamic Surface Configuration.....	5
4	Root Roll Response Using Trapezoidal Integration Technique....	7
5	Root Pitch Response Using Trapezoidal Integration Technique...	8
6	Simulation Results for Rigid Aerodynamic Surface with Root Roll Preload Nonlinearity.....	18
7	Simulation Results for Rigid Aerodynamic Surface with Root Pitch Preload Nonlinearity.....	19
8	Root Roll Simulation Results for a Flexible Aerodynamic Surface with Two Preload Nonlinearities.....	21
9	Root Pitch Simulation Results for a Flexible Aerodynamic Surface with Two Preload Nonlinearities.....	22
10	Aerodynamic Surface Response for a Dynamic Pressure of 50 psi.	24
11	Root Roll PSD for a Dynamic Pressure of 50 psi.....	25
12	Frequency Content of Root Roll Response Versus Dynamic Pressure.....	26
13	Lowest Two Frequency Components as a Function of Dynamic Pressure.....	27
14	Aerodynamic Surface Response for a Dynamic Pressure of 70 psi.	28
15	Root Roll PSD for a Dynamic Pressure of 70 psi.....	29
16	Comparison of Computational Efficiency for Numerical Integration Techniques.....	32
17	Region of Correlation Anomaly.....	34
A1	Aerodynamic Surface Geometry.....	38
A2	Aerodynamic Surface Inertia Properties.....	39
A3	Aerodynamic Surface Cantilever Modes.....	40

## LIST OF SYMBOLS

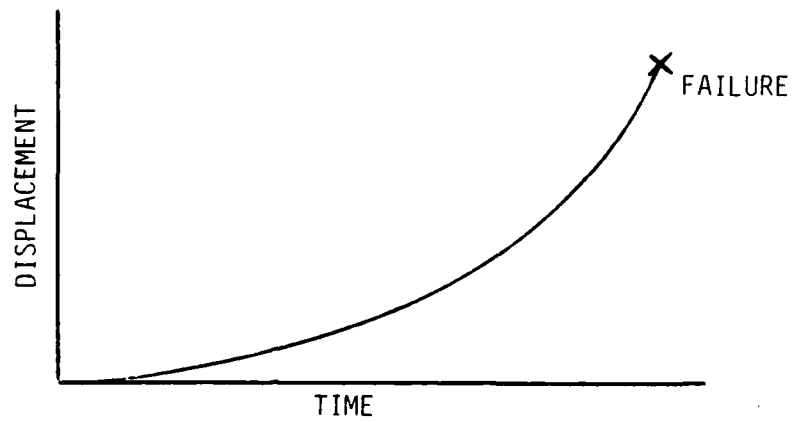
A	Amplitude of motion at surface root support
B	Elements of aerodynamic forcing function matrix
D	State variable dynamic matrix
h	Numerical integration step size
I	Rigid aerodynamic surface inertia
K(X)	Spring rate of root springs
M	System mass
$m_n$	Flexible aerodynamic surface generalized masses
P	Preload parameter
PF	Aerodynamic surface participation factors
Q	Aerodynamic matrix for state variable formulation
q	Dynamic pressure
$q_n$	Flexible aerodynamic surface generalized coordinates
S	Deadspace
t	Time
X	Matrix of aerodynamic surface degrees of freedom
Y	Matrix of aerodynamic surface state variables
$\phi$	Displacement in root pitch
$\theta$	Displacement in root roll
$\omega_\phi, \omega_\theta$	Uncoupled natural frequencies of linearized system
$\omega_n$	Flexible aerodynamic surface natural frequencies
<u>Subscripts</u>	
A...K	Indicies associated with intermediate numerical integration time steps
n	Indicies associated with numerical integration time step
$\phi$	Associated with root pitch degree of freedom
$\theta$	Associated with root roll degree of freedom

## 1.0 INTRODUCTION

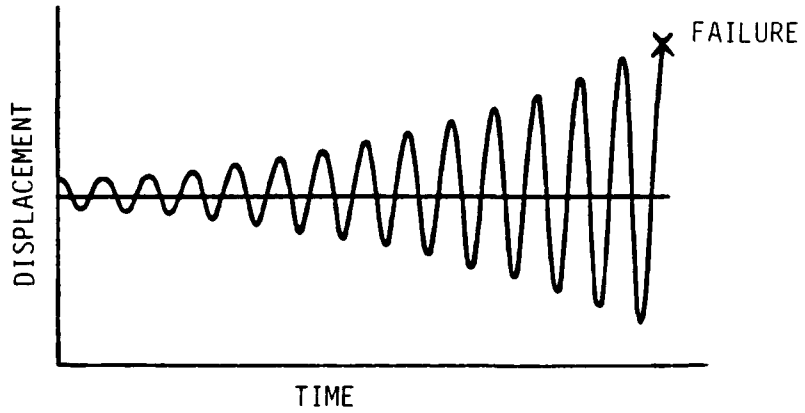
Defining the flutter and divergence characteristics of aerodynamic surfaces is a basic requirement in assuring structural and performance integrity of a given design for its operational environment. The response characteristics of the divergence and flutter phenomena are illustrated in Figures 1(a) and (b). For systems containing structural nonlinearities, another mode of aeroelastic response--limit cycle oscillation--may be present. Limit cycle response, Figure 1(c), is characterized by steady state oscillation whereas divergence and flutter are unstable motions with increasing amplitude. The potential of limit cycle response is of importance since these oscillations may occur within the aerosurface flutter and divergence flight envelope. The amplitude, frequency, and duration of these potential limit cycle oscillations are of interest for a fatigue assessment of the system.

Frequently aerodynamic surface hardware designs do have nonlinearities in the surface itself, support structure, and/or control actuators as a result of manufacturing tolerances, design characteristics, and/or freeplay. When these nonlinearities exist, the assumption of a linear force-displacement relationship is no longer justified. In this situation an understanding of the nonlinear effect on the dynamic behavior is required to evaluate system response.

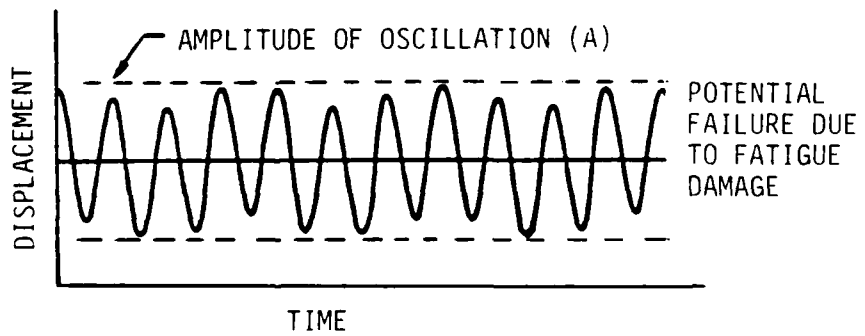
The effects of structural nonlinearities on aeroelastic analysis have been studied both analytically and experimentally, Reference 1 through 9. In these studies several nonlinearities that are typically encountered in aerodynamic surface designs were considered. The primary thrust of the early work attempted to establish a basic understanding of the nonlinear system response employing analog computers. The later analytical studies, References 4 and 6, employed the describing function techniques to characterize the nonlinear behavior of an aerodynamic surface. A majority of the work addressed freeplay nonlinearities of the type shown in Figure 2. These nonlinearities are representative of a deadband or "slop" in the root support structure of an



(a) - DIVERGENCE



(b) - FLUTTER



(c) - LIMIT CYCLE

FIGURE 1 MODES OF AERODYNAMIC SURFACE AEROELASTIC RESPONSE

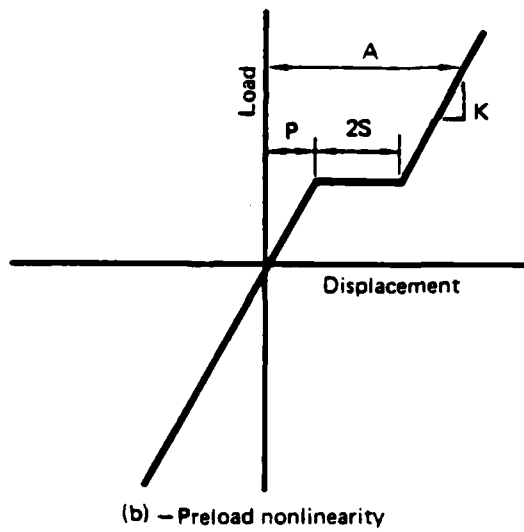
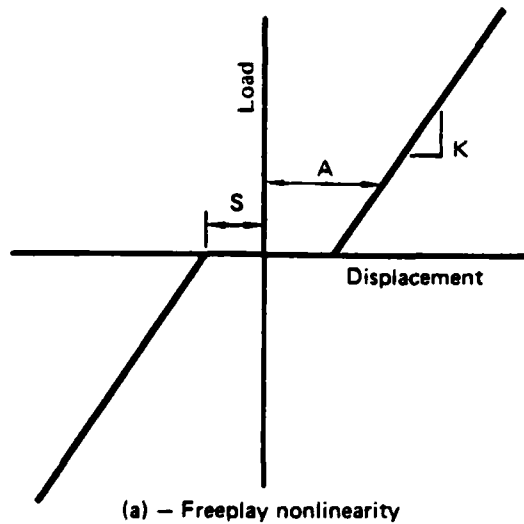


FIGURE 2 TYPES OF STRUCTURAL NONLINEARITIES

aerodynamic surface with and without a preload. The approach discussed in Reference 5 is a procedure in the frequency domain which iteratively obtains a consistent solution in terms of response amplitude and effective stiffness of the nonlinear structural element.

The describing function approach, References 4 and 6, uses a one term Fourier Series expansion of the force to account for the effect of the nonlinear stiffness on aerodynamic surface response. This method yields satisfactory results when the amplitude of displacement is greater than the magnitude of the freeplay, Figure 2(a), or freeplay plus preload, Figure 2(b). However, it was pointed out in References 4 and 6 that when the amplitude of displacement is approximately equal to the magnitude of the nonlinearity, significant error can occur as a result of neglecting the higher harmonics in the series expansion of the force-displacement relationship.

An analytical study sponsored by AFOSR was undertaken, Reference 9, to develop an improved technique for predicting limit cycle response of aerodynamic surfaces with discrete structural nonlinearities. This improved technique was to retain the flexibility of the describing function approach while providing greater accuracy and generality in modeling the nonlinear system behavior. An asymptotic expansion method was developed to model the nonlinear force-displacement relationship that results when nonlinearities of the type shown in Figure 2 are introduced at the aerodynamic surface support. The primary difference between the asymptotic method and the describing function method is the capability of the asymptotic method to include higher harmonics in the representation of the system nonlinearity. In this manner one may obtain successively higher order approximations to the limit cycle response.

Specifically, the problem investigated during the Reference 9 study was the limit cycle response of an aerodynamic surface in a subsonic airstream, Figure 3. The nonlinearities shown in Figure 2 were assumed to act at the root support springs  $K_\phi$  and  $K_\theta$  of the structure. This problem is representative of a control surface with a loose hinge and/or joint slippage in the surface

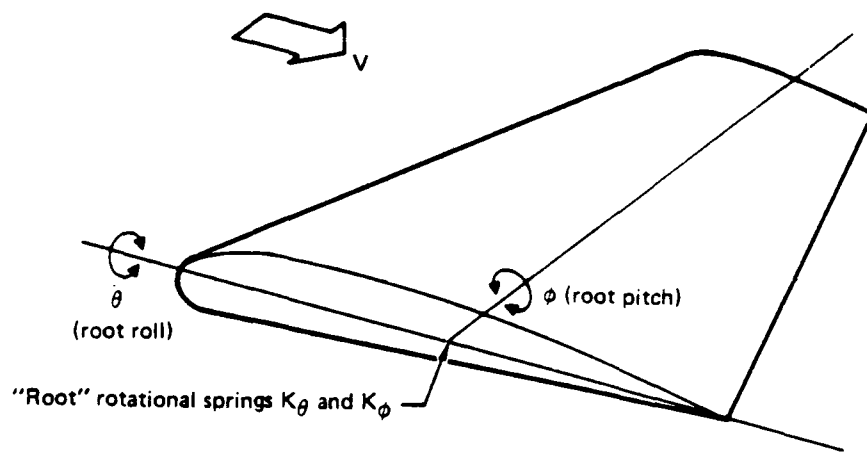


FIGURE 3 AERODYNAMIC SURFACE CONFIGURATION

support structure and/or control actuator. The aerodynamic forces acting on the surface were modeled using steady state aerodynamic theory. This theory assumes the lifting force is proportional to and in phase with the torsional motion of the surface which is assumed to be sinusoidal. Simple aerodynamics were assumed since the primary objective of this previous study was the investigation of the influence of structural nonlinearities on aerodynamic surface response. As discussed in Reference 6, use of a more sophisticated aerodynamic theory can substantially change the linear flutter results employed to predict nonlinear aeroelastic response, but has no impact on interpretation of the system response behavior due to the presence of structural nonlinearities.

During the Reference 9 study, numerical simulation results were used to evaluate the adequacy of the asymptotic expansion technique. The "exact" solutions for aerodynamic surface response were obtained via numerical integration of the system nonlinear equations of motion. These "exact" solutions were then compared with the asymptotic expansion predictions to assess the accuracy of these predictions. The numerical simulation approach employed during this previous investigation was based on a "simple" trapezoidal integration method, Reference 10.

It became apparent during the Reference 9 investigations that there were situations when the trapezoidal simulation technique exhibited numerical stability problems. Examples of the results observed during the Reference 9 study are shown in Figures 4 and 5. Here simulation results employing the trapezoidal integration technique are compared with the asymptotic expansion results of Reference 9. This example is for a flexible aerodynamic surface having preload nonlinearities in both root degrees of freedom. The differences in simulation results when compared to the approximate solution may be noted. These differences indicate that the trend of simulation results do not correspond to those of the asymptotic expansion technique. Due to the "scatter" of the simulation results, the accuracy of these results was in question.

- o FLEXIBLE AERODYNAMIC SURFACE
- o TWO PRELOAD NONLINEARITIES
  - $S_\phi = S_\theta = 0.2 \text{ deg}$
  - $P_\phi = P_\theta = 0.1 \text{ deg}$
- o UNCOUPLED FREQUENCIES
  - $\omega_\phi = 215 \text{ Hz}$
  - $\omega_\theta = 60 \text{ Hz}$

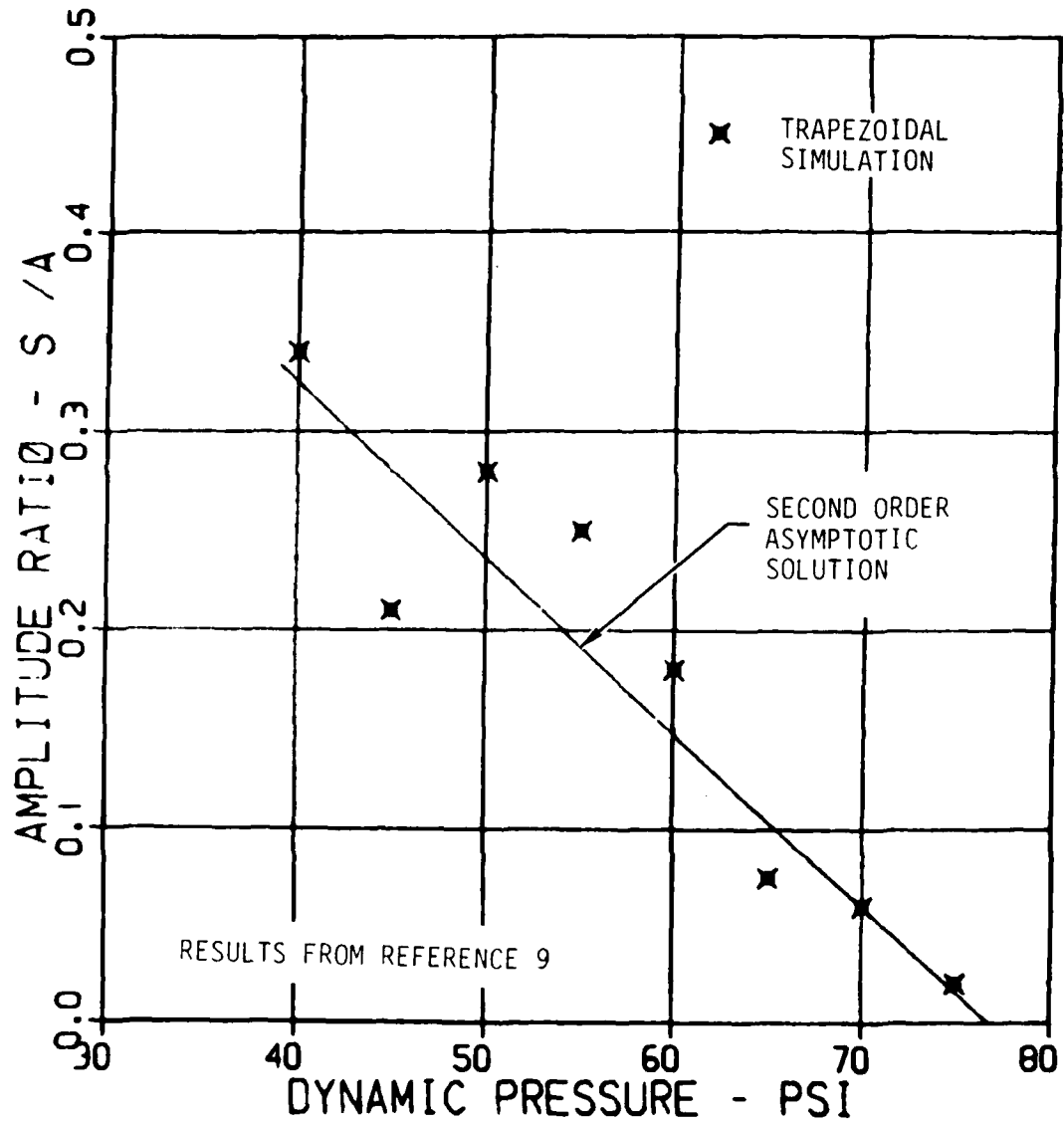


FIGURE 4 ROOT ROLL RESPONSE USING TRAPEZOIDAL INTEGRATION TECHNIQUE

- o FLEXIBLE AERODYNAMIC SURFACE
- o TWO PRELOAD NONLINEARITIES
  - $S_\phi = S_\theta = 0.2 \text{ deg}$
  - $P_\phi = P_\theta = 0.1 \text{ deg}$
- o UNCOUPLED FREQUENCIES
  - $\omega_\phi = 215 \text{ Hz}$
  - $\omega_\theta = 60 \text{ Hz}$

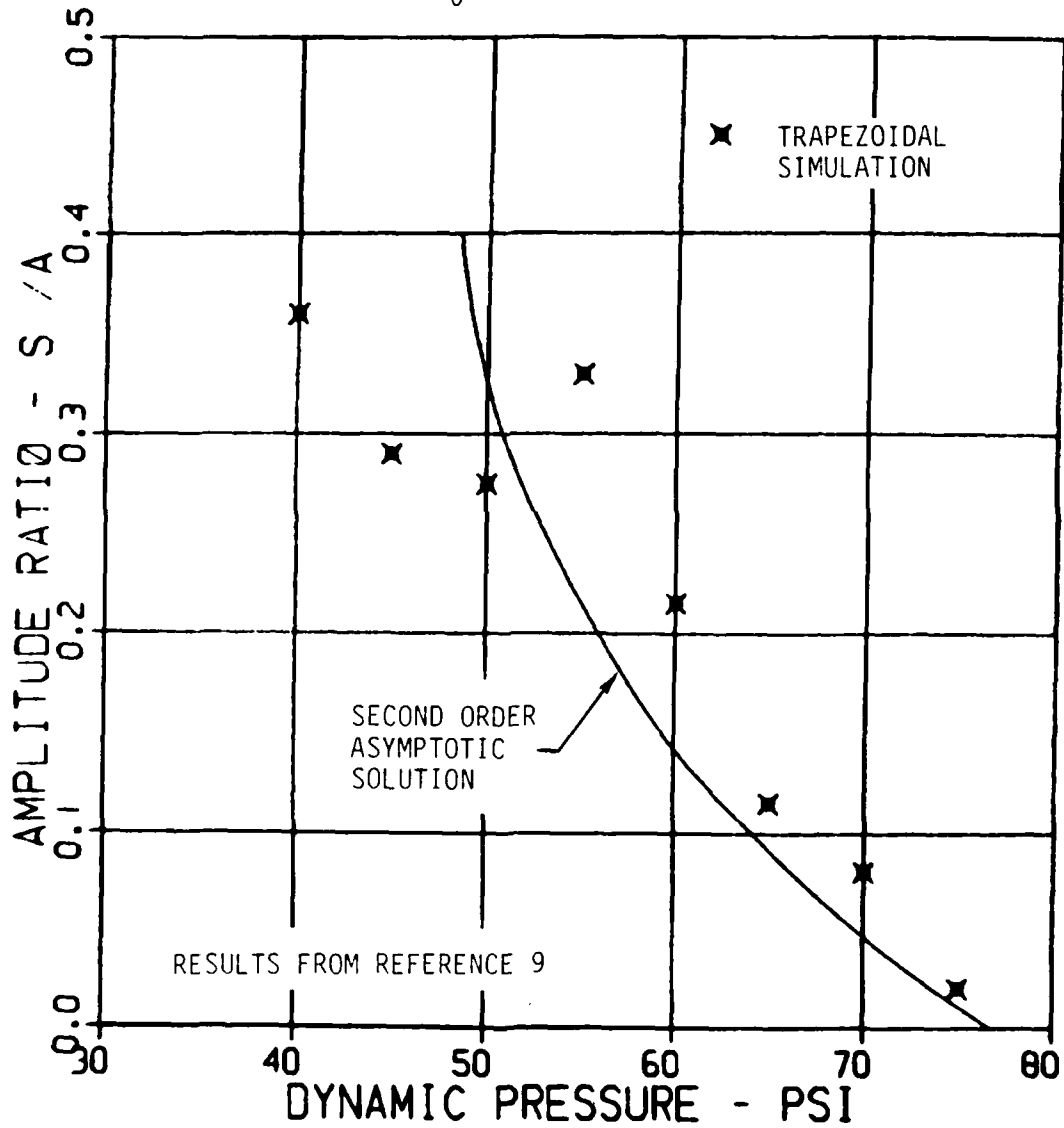


FIGURE 5 ROOT PITCH RESPONSE USING TRAPEZOIDAL INTEGRATION TECHNIQUE

Thus, the present study was undertaken to evaluate these simulation shortcomings. The objective of this study was to evaluate, on a comparative basis, more refined numerical simulation techniques for predicting the response of aerodynamic surfaces containing discrete structural nonlinearities. During this study the suitability of three different type numerical simulation techniques were compared in terms of predicting the large amplitude limit cycles oscillations of a nonlinear aerodynamic surface. The three numerical techniques investigated were:

- Runge-Kutta
- Shanks
- Adams-Moulton

Details of these numerical integration techniques are presented in Section 2.0. This is followed, Section 3.0, by the numerical results obtained for the three numerical procedures. These results are compared with both the data obtained via the trapezoidal integration routine and the asymptotic expansion approach of Reference 9. Study conclusions are presented in Section 4.0.

## 2.0 NUMERICAL INTEGRATION TECHNIQUES

The objective of this present study was to evaluate, on a comparative basis, different numerical simulation approaches for predicting limit cycle response of aerodynamic surfaces containing discrete structural nonlinearities. The nonlinear equations of motion of interest are of the form

$$M \ddot{X} + K(X) X = q B X \quad (1)$$

These system of equations govern the nonlinear aeroelastic response of the aerodynamic surface configuration shown in Figure 1. The detailed elements of Equation (1) are given as:

$$\begin{bmatrix} I_{\theta} & I_{\theta\phi} & & \\ I_{\phi\theta} & I_{\phi} & & \\ & & PF & \\ & & & m_n \end{bmatrix} \begin{bmatrix} \ddot{\theta} \\ \ddot{\phi} \\ \ddot{q}_n \end{bmatrix} + \begin{bmatrix} K(\theta) & 0 & & \\ 0 & K(\phi) & & \\ & & & 0 \\ & & & m_n \omega_n^2 \end{bmatrix} \begin{bmatrix} \theta \\ \phi \\ q_n \end{bmatrix} = q \begin{bmatrix} B_r & B_{re} \\ & \\ B_{er} & B_e \end{bmatrix} \begin{bmatrix} \theta \\ \phi \\ q_n \end{bmatrix} \quad (2)$$

For this study, and the previous investigations of References 4, 6 and 9, a baseline aerodynamic surface was assumed for evaluating the coefficients of Equation (2). This baseline configuration was based on the Harpoon Anti-Ship missile quick-attach control surface. Details of this aerodynamic surface may be found in Appendix A.

Three numerical integration techniques were chosen for evaluation during this study. These were: (1) a fourth-order Runge-Kutta method, (2) an eighth-order Shanks method, and (3) a fourth-order Adams-Moulton predictor-corrector method. Each method was used to obtain time history solutions for the equations of motion. Equation (1), of an aerodynamic surface containing discrete structural nonlinearities.

All three methods required that the second order equations of Equation (1) be transformed to first order equations using an appropriate state variable transformation. Thus, Equation (1) was expressed as:

$$\dot{Y} + D(Y) Y = Q Y \quad (3)$$

where

$$Y = \begin{pmatrix} \dot{X} \\ X \end{pmatrix} \quad (4)$$

The matrices  $D(Y)$  and  $Q$  of Equation (4) are of the form

$$D(Y) = \begin{bmatrix} 0 & ; & M^{-1}K(X) \\ -I & ; & 0 \end{bmatrix} \quad (5)$$

and

$$Q = \begin{bmatrix} 0 & ; & q M^{-1}B \\ 0 & ; & 0 \end{bmatrix} \quad (6)$$

where  $I$  is the identity matrix and the remaining terms correspond to elements of Equation (1).

The following notation is used to present the specific form of each numerical integration technique. For the initial value problem

$$\dot{Y} = f(Y, t), Y(t_0) = Y_0 \quad (7)$$

at any step  $n$  in the calculation, the available quantities are

$$t_n, Y_n \text{ and } \dot{Y}_n = f(Y_n, t_n) \quad (8)$$

Referring to Equation (3) the quantity  $f(Y_n, t_n)$  is defined as

$$f(Y_n, t_n) = Q Y_n - D(Y_n) Y_n \quad (9)$$

For an integration step size set equal to  $h$  we have

$$t_{n+1} = t_n + h \quad (10)$$

and the numerical integration procedure computes a value for  $Y_{n+1}$ . The quantity

$$\dot{Y}_{n+1} = f(Y_{n+1}, t_{n+1}) \quad (11)$$

is then calculated and the integration cycle is repeated.

Each of the three numerical integration procedures used during this study are described in detail in the following sections.

### 2.1 Fourth-Order Runge-Kutta

The Runge-Kutta integration method, Reference 11, was selected for this study because it is a basic, widely used constant step integration technique. This method uses the following procedure to compute  $Y_{n+1}$ . First, the sequence of computations given below are performed:

$$\begin{aligned} Y_A &= Y_n + (h/2) \dot{Y}_n \\ \dot{Y}_A &= f(\dot{Y}_A, t_n + h/2) \\ Y_B &= Y_n + (h/2) \dot{Y}_A \\ \dot{Y}_B &= f(\dot{Y}_B, t_n + h/2) \\ Y_C &= Y_n + h \dot{Y}_B \\ \dot{Y}_C &= f(\dot{Y}_C, t_n + h) \end{aligned} \quad (12)$$

Then  $Y_{n+1}$  at time  $t_{n+1}$  is defined as:

$$Y_{n+1} = Y_n + (h/6) (\dot{Y}_n + 2\dot{Y}_A + 2\dot{Y}_B + \dot{Y}_C) \quad (13)$$

## 2.2 Eighth-Order Shanks

The eighth-order Shanks constant step integration approach, Reference 12, was selected as a means to incorporate a higher order method of the Runge-Kutta type approach in the simulation. This was of interest to study the effects of reducing the truncation error inherent to these integration methods. To obtain an estimate of  $Y_{n+1}$ , first the following sequence of calculations are made:

$$\begin{aligned} Y_A &= Y_n + (h/9) \dot{Y}_n \\ \dot{Y}_A &= f(Y_A, t_n + h/9) \\ Y_B &= Y_n + (h/24) (\dot{Y}_n + 3\dot{Y}_A) \\ \dot{Y}_B &= f(Y_B, t_n + h/6) \\ Y_C &= Y_n + (h/16) (\dot{Y}_n + 3\dot{Y}_B) \\ \dot{Y}_C &= f(Y_C, t_n + h/4) \\ Y_D &= Y_n + (h/500) (29\dot{Y}_n + 33\dot{Y}_B - 12\dot{Y}_C) \\ \dot{Y}_D &= f(Y_D, t_n + h/10) \\ Y_E &= Y_n + (h/972) (33\dot{Y}_n + 4\dot{Y}_C + 125\dot{Y}_D) \\ \dot{Y}_E &= f(Y_E, t_n + h/6) \end{aligned} \quad (14)$$

$$Y_F = Y_n + (h/36) (-21\dot{Y}_n + 76\dot{Y}_C + 125\dot{Y}_D - 162\dot{Y}_E)$$

$$\dot{Y}_F = f(Y_F, t_n + h/2)$$

$$Y_G = Y_n + (h/243) (-30\dot{Y}_n - 32\dot{Y}_C + 125\dot{Y}_D + 99\dot{Y}_F)$$

$$\dot{Y}_G = f(Y_G, t_n + 2h/3)$$

$$Y_H = Y_n + (h/324) (1175\dot{Y}_n - 3456\dot{Y}_C - 6250\dot{Y}_D \\ + 8424\dot{Y}_E + 242\dot{Y}_F - 27\dot{Y}_G)$$

$$\dot{Y}_H = f(Y_H, t_n + h/3)$$

$$Y_I = Y_n + (h/324) (293\dot{Y}_n - 852\dot{Y}_C - 1375\dot{Y}_D + 1836\dot{Y}_E \\ - 118\dot{Y}_F + 162\dot{Y}_G + 324\dot{Y}_H)$$

(14)

CONTINUED

$$\dot{Y}_I = f(Y_I, t_n + 5h/6)$$

$$Y_J = Y_n + (h/1620) (1303\dot{Y}_n - 4260\dot{Y}_C - 6875\dot{Y}_D \\ + 9990\dot{Y}_E + 1030\dot{Y}_F + 162\dot{Y}_I)$$

$$\dot{Y}_J = f(Y_J, t_n + 5h/6)$$

$$Y_K = Y_n + (h/4428) (-8595\dot{Y}_n + 30720\dot{Y}_C + 48750\dot{Y}_D \\ - 66096\dot{Y}_E + 378\dot{Y}_F - 729\dot{Y}_G - 1944\dot{Y}_H - 1296\dot{Y}_I + 3240\dot{Y}_J)$$

$$\dot{Y}_K = f(Y_K, t_n + h)$$

The value for  $Y_{n+1}$  at a time  $t_{n+1}$  is then obtained from:

$$Y_{n+1} = Y_n + (h/840) (41\dot{Y}_n + 216\dot{Y}_E + 272\dot{Y}_F + 27\dot{Y}_G + 27\dot{Y}_H + 36\dot{Y}_I + 180\dot{Y}_J + 41\dot{Y}_K) \quad (15)$$

### 2.3 Fourth-Order Adams-Moulton

The Adams-Moulton integration technique, Reference 11, was also included in this study. This technique was selected since it is a predictor-corrector procedure and thus computationally very different from the previous two methods. The Adams-Moulton procedure uses the following sequence of computations to calculate  $Y_{n+1}$ . The predicted value at  $t_{n+1}$  is

$$P_{n+1} = Y_n + (h/24) (55\dot{Y}_n - 59\dot{Y}_{n-1} + 37\dot{Y}_{n-2} - 9\dot{Y}_{n-3}) \quad (16)$$

The corrected value at  $t_{n+1}$  is then given as

$$C_{n+1} = Y_n + (h/24) (9\dot{P}_{n+1} + 19\dot{Y}_n - 5\dot{Y}_{n-1} + \dot{Y}_{n-2}) \quad (17)$$

where

$$\dot{P}_{n+1} = f(P_{n+1}, t_{n+1}) \quad (18)$$

and

$$Y_{n+1} = C_{n+1} + (19/270) (P_{n+1} - C_{n+1}) \quad (19)$$

The predicted and corrected values are used to evaluate an accuracy indicator defined as

$$E_n = \max[\min(|P_n^i - C_n^i|, |(P_n^i - C_n^i)/C_n^i|)] \quad (20)$$

for  $i = 1, 2, 3, \dots, N$

In Equation (20),  $N$  is the total number of integrated variables and  $i$  denotes the  $i^{\text{th}}$  integrated variable.

The parameter  $E_n$  is then compared to two constants,  $E_{\min}$  and  $E_{\max}$ , and  $h$  is varied as follows:

- (1) If  $E_{n-j} < E_{\min}$  ( $j = 0, 1, 2, \text{ or } 3$ );  $h$  is doubled and the integration is restarted.
- (2) If  $E_{\min} \leq E_n \leq E_{\max}$ ,  $h$  is left unchanged.
- (3) If  $E_n \geq E_{\max}$ ;  $h$  is halved and the integration is restarted.

For these studies  $E_{\min}$  was set at  $5 \times 10^{-9}$  and  $E_{\max}$  at  $5 \times 10^{-6}$ . These values were selected based on information provided in Reference 13.

As can be seen from Equations (16) and (17), the Adams-Moulton method is not self-starting. Each time the integration is started (restarted), the Runge-Kutta technique is used to compute the first three points. The Adams-Moulton procedure is then used until a restart becomes necessary.

### 3.0 NUMERICAL SIMULATION RESULTS

Numerical simulation results were obtained for the aerodynamic surface nonlinear equations of motion, Equation (1), for each of the three integration techniques discussed in Section 2.0. The results from each numerical approach, for a uniform set of physical parameters, were compared with each other to evaluate the relative accuracy in predicting the system steady state limit cycle response. These numerical solutions were obtained for both a rigid and a flexible aerodynamic surface. However, a majority of the study effort was directed toward a flexible aerodynamic surface with two preload nonlinearities. This configuration was of primary interest since the results of References 4 and 9 concluded that the poorest correlation between the approximate solutions and simulation results was observed for this case.

Power Spectral Density (PSD) analysis studies were also performed to determine the frequency content of the time history simulation results. This frequency content information is of interest when interpreting the numerical simulation results. As discussed in Section 3.2, review of the frequency information provided insight into the changing nature of the nonlinear system response as a function of varying dynamic pressure.

#### 3.1 Rigid Aerodynamic Surface

Results of the numerical simulations for the rigid aerodynamic surface are shown in Figure 6 and 7. Shown here are the numerically predicted limit cycle amplitudes of response as a function of dynamic pressure. For both cases, it was assumed that the uncoupled root roll frequency ( $\omega_\theta$ ) was 60 Hz and the pitch frequency ( $\omega_\phi$ ) was 215 Hz. The results in Figure 6 are for a preload nonlinearity in the root roll degree of freedom, while Figure 7 results are for a root pitch preload nonlinearity. In each case the nonlinearity was defined by a deadspace (S) of 0.2 degrees and a preload (P) of 0.1 degrees. Thus the S over P ratio, see Figure 2, was two for both cases.

- o RIGID AERODYNAMIC SURFACE
- o ROLL PRELOAD NONLINEARITY
  - $S_{\theta} = 0.2$  deg
  - $P_{\theta} = 0.1$  deg
- o UNCOUPLED FREQUENCIES
  - $\omega_{\phi} = 215$  Hz
  - $\omega_{\theta} = 60$  Hz

DYNAMIC PRESSURE (psi)	AMPLITUDE RATIO (S/A)		
	RUNGE-KUTTA	SHANKS	ADAMS-MOULTON
40	0.34357	0.34357	0.34357
60	.31363	.31363	.31363
80	.31139	.31139	.31139
90	.11181	.11181	.11181
95	.05171	.05165	.05164

FIGURE 6 SIMULATION RESULTS FOR RIGID AERODYNAMIC SURFACE WITH ROOT ROLL PRELOAD NONLINEARITY

- o RIGID AERODYNAMIC SURFACE
- o PITCH PRELOAD NONLINEARITY
  - $S_{\phi} = 0.2$  deg
  - $P_{\phi} = 0.1$  deg
- o UNCOUPLED FREQUENCIES
  - $\omega_{\phi} = 215$  Hz
  - $\omega_{\theta} = 60$  Hz

DYNAMIC PRESSURE (psi)	AMPLITUDE RATIO (S/A)		
	RUNGE-KUTTA	SHANKS	ADAMS-MOULTON
40	0.35331	0.35295	0.35295
50	.27660	.27682	.27682
70	.15124	.15131	.15243
90	.02935	.02940	.02944

FIGURE 7 SIMULATION RESULTS FOR RIGID AERODYNAMIC SURFACE WITH ROOT PITCH PRELOAD NONLINEARITY

As can be seen by the data presented in Figures 6 and 7, the results from the three integration procedures compared very well with each other and yield essentially identical results. It should be noted that the computational time was quite different for the three methods. This point is discussed in more detail in Section 4.0.

### 3.2 Flexible Aerodynamic Surface

The numerical simulation results for a flexible aerodynamic surface are presented in Figures 8 and 9. These simulation results, amplitude ratio versus dynamic pressure, are also compared to asymptotic expansion results of Reference 9. The Reference 9 simulation results, employing the trapezoidal procedure are also shown for comparative purposes.

The results presented in these figures correspond to an aerodynamic surface with preload nonlinearities in both root degrees of freedom. In each case the deadspace (S) is 0.2 degrees and the preload (P) is 0.1 degrees. Thus the preload ratio (S/P) is two for both nonlinearities. In addition, the uncoupled root roll frequency ( $\omega_\theta$ ) was 60 Hz and the pitch frequency ( $\omega_\phi$ ) was 215 Hz.

Several points are evident from the data shown in Figure 8 and 9. First, the three integration techniques yield similar magnitudes of limit cycle amplitude ratios for a given set of physical parameters. Additionally, this similarity of results is consistent over a wide range of dynamic pressures and associated large range of limit cycle response amplitudes. In general the results obtained with the refined simulation techniques show improved correlation with the asymptotic expansion results when compared to the results obtained via the trapezoidal integration scheme.

However, there remain regions where the comparison between the refined numerical simulations and approximate solutions is inconclusive. To more fully evaluate these regions of inconsistent results, frequency analyses were

- o FLEXIBLE AERODYNAMIC SURFACE
- o TWO PRELOAD NONLINEARITIES
  - $S_\phi = S_\theta = 0.2 \text{ deg}$
  - $P_\phi = P_\theta = 0.1 \text{ deg}$
- o UNCOUPLED FREQUENCIES
  - $\omega_\phi = 215 \text{ Hz}$
  - $\omega_\theta = 60 \text{ Hz}$

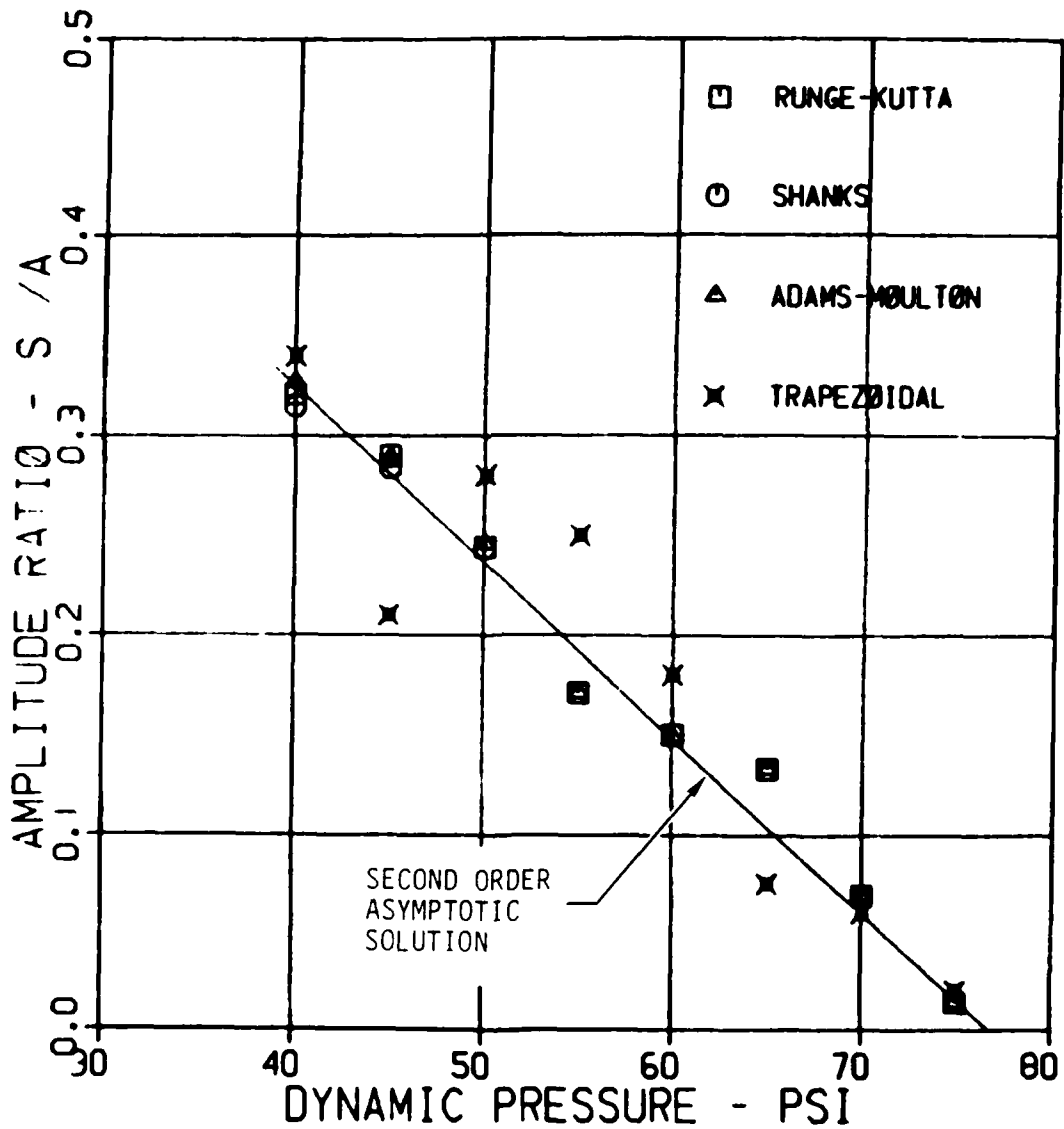


FIGURE 8 ROOT ROLL SIMULATION RESULTS FOR A FLEXIBLE AERODYNAMIC SURFACE WITH TWO PRELOAD NONLINEARITIES

- o FLEXIBLE AERODYNAMIC SURFACE
- o TWO PRELOAD NONLINEARITIES
  - $S_\phi = S_\theta = 0.2 \text{ deg}$
  - $P_\phi = P_\theta = 0.1 \text{ deg}$
- o UNCOUPLED FREQUENCIES
  - $\omega_\phi = 215 \text{ Hz}$
  - $\omega_\theta = 60 \text{ Hz}$

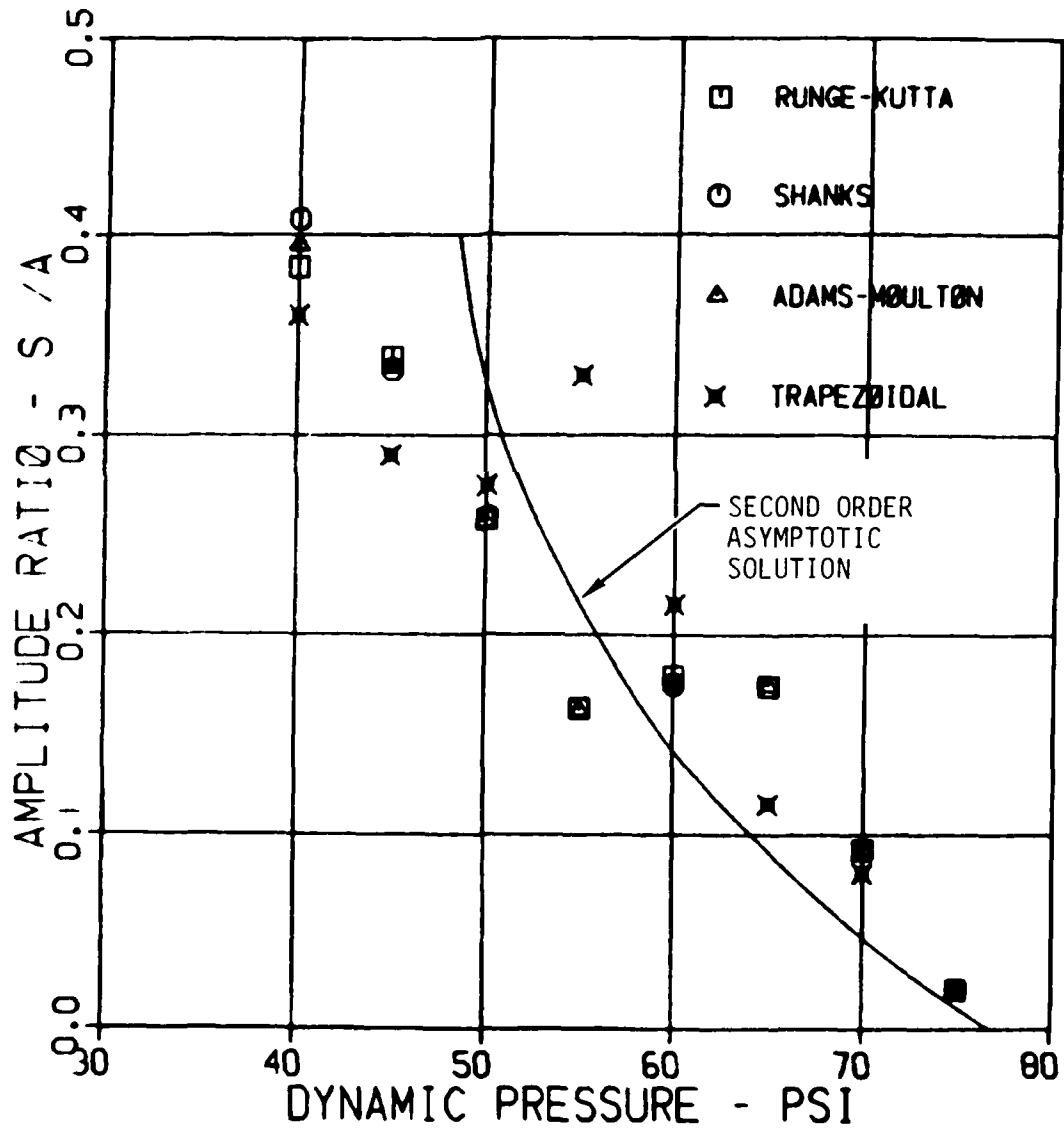


FIGURE 9 ROOT PITCH SIMULATION RESULTS FOR A FLEXIBLE AERODYNAMIC SURFACE WITH TWO PRELOAD NONLINEARITIES

performed on the simulation developed time history response data. This was done in an attempt to more completely define the mechanism of aerodynamic surface dynamic response in these regions.

These investigations of response frequency content were done by first performing PSD analyses of the root degrees of freedom displacement data. As an example, time history data for the root degrees of freedom and a dynamic pressure of 50 psi are shown in Figure 10. The corresponding roll response PSD, ( $\text{radians}^2/\text{Hz}$  versus Hz) is shown in Figure 11.

From data such as shown in Figure 11, the frequency content of the system response was obtained. This was accomplished by noting the frequencies associated with the peak or highest values of PSD. A summary of these results is given in Figure 12 for response in the root roll degree of freedom over a wide range of dynamic pressures. The highest two frequency components remain essentially constant over the range of dynamic pressures evaluated. As may be seen from Figure 12, there is significant change in the lowest two frequencies with changing dynamic pressure. Time history information from which the data presented in Figure 12 were derived are presented in Appendix B.

These lowest two frequencies are plotted as a function of dynamic pressure in Figure 13. Note that these frequencies are the average values for the root pitch and root roll response. There was some slight difference in the frequencies obtained from the roll and pitch PSD's. The trend shown in Figure 13 is similar to the classic frequency coalescence of a linear system flutter analysis.

It is of interest to note that there is a change in the nature of the limit cycle response as the dynamic pressure approaches the linear system flutter boundary. This change in response characteristics may be seen by comparing the results shown in Figures 14 and 15, for a dynamic pressure of 70 psi, with that of Figures 10 and 11 for a dynamic pressure of 50 psi. As can be seen in Figure 14, the root displacement has developed a beat type characteristic. This is further manifested by the PSD results of Figure 15. From the data in

- o FLEXIBLE AERODYNAMIC SURFACE
- o TWO PRELOAD NONLINEARITIES
  - $S_{\phi} = S_{\theta} = 0.2$  deg
  - $P_{\phi} = P_{\theta} = 0.1$  deg
- o UNCOUPLED FREQUENCIES
  - $\omega_{\phi} = 215$  Hz
  - $\omega_{\theta} = 60$  Hz

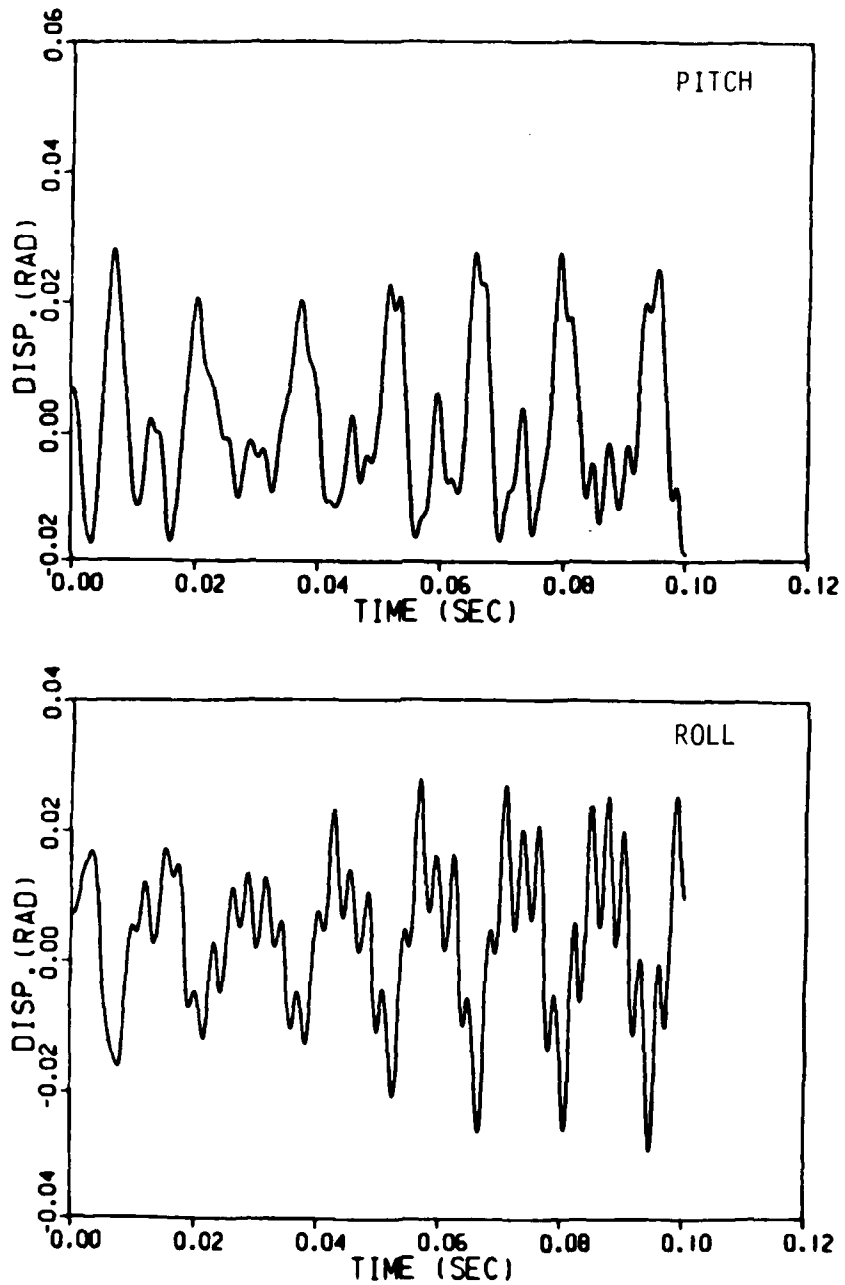


FIGURE 10 AERODYNAMIC SURFACE RESPONSE FOR A DYNAMIC PRESSURE OF 50 PSI

o FLEXIBLE AERODYNAMIC SURFACE

o TWO PRELOAD NONLINEARITIES

$$S_{\phi} = S_{\theta} = 0.2 \text{ deg}$$

$$P_{\phi} = P_{\theta} = 0.1 \text{ deg}$$

o UNCOUPLED FREQUENCIES

$$\omega_{\phi} = 215 \text{ Hz}$$

$$\omega_{\theta} = 60 \text{ Hz}$$

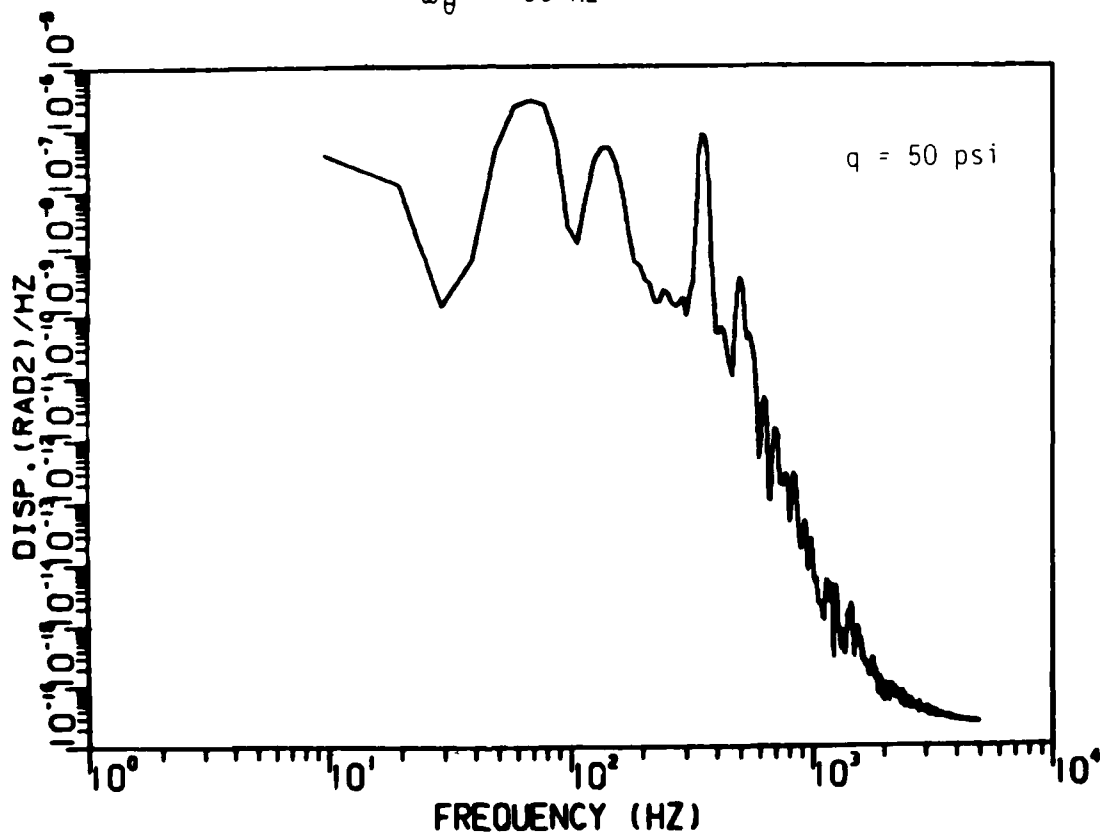


FIGURE 11 ROOT ROLL PSD FOR A DYNAMIC PRESSURE OF 50 PSI

- o FLEXIBLE AERODYNAMIC SURFACE
- o TWO PRELOAD NONLINEARITIES
  - $S_{\phi} = S_{\theta} = 0.2 \text{ deg}$
  - $P_{\phi} = P_{\theta} = 0.1 \text{ deg}$
- o UNCOUPLED FREQUENCIES
  - $\omega_{\phi} = 215 \text{ Hz}$
  - $\omega_{\theta} = 60 \text{ Hz}$

Dynamic Pressure (psi)	Frequency Components (Hz)			
	1st	2nd	3rd	4th
40	55	140	350	500
45	65	140	350	500
50	70	140	350	500
55	70	130	350	500
60	72	130	350	500
65	80	110	340	500
70	100	100	340	500
75	110	110	350	500

FIGURE 12 FREQUENCY CONTENT OF ROOT ROLL RESPONSE VERSUS DYNAMIC PRESSURE

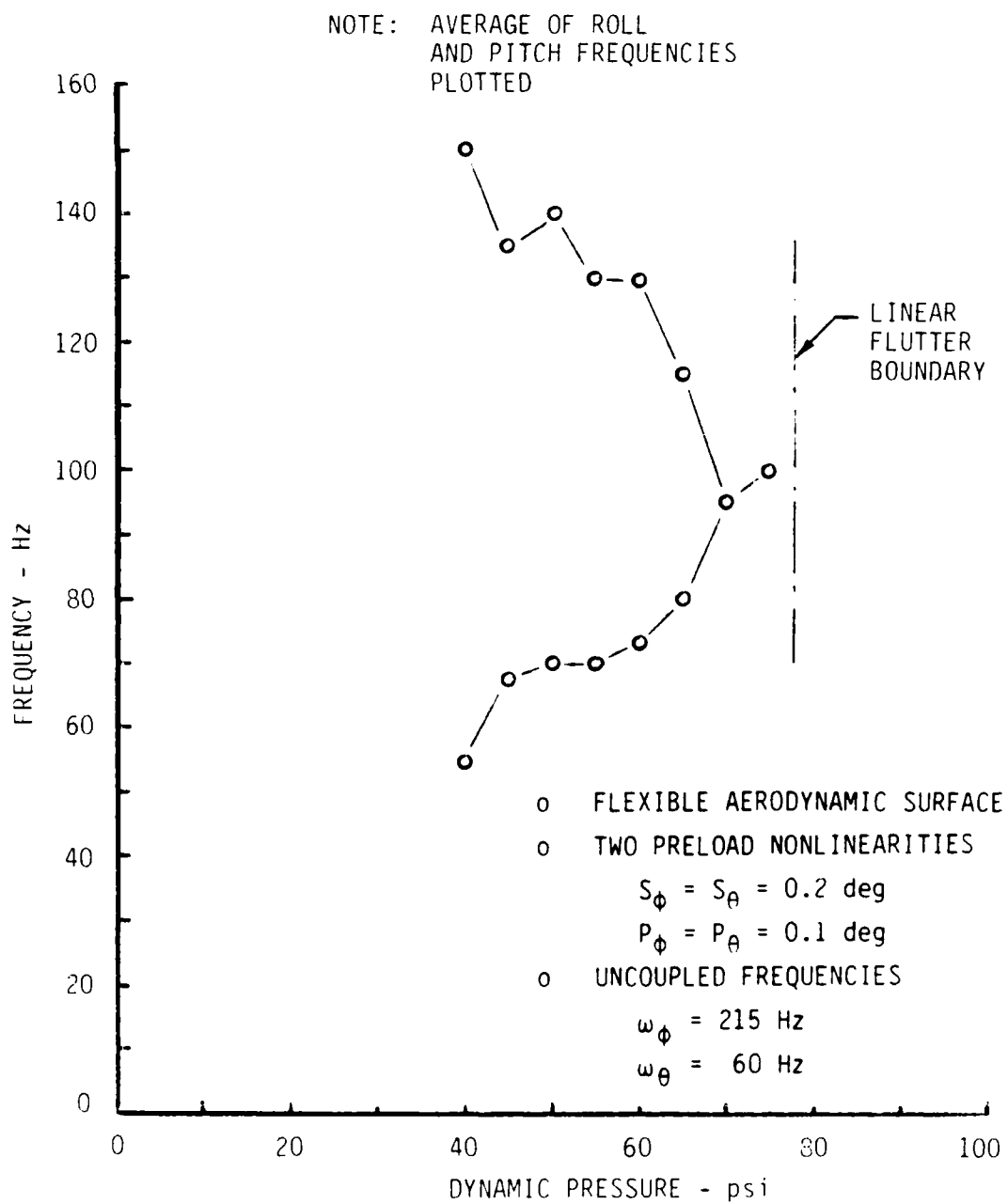


FIGURE 13 LOWEST TWO FREQUENCY COMPONENTS AS A FUNCTION OF DYNAMIC PRESSURE

- o FLEXIBLE AERODYNAMIC SURFACE
- o TWO PRELOAD NONLINEARITIES
  - $S_\phi = S_\theta = 0.2 \text{ deg}$
  - $P_\phi = P_\theta = 0.1 \text{ deg}$
- o UNCOUPLED FREQUENCIES
  - $\omega_\phi = 215 \text{ Hz}$
  - $\omega_\theta = 60 \text{ Hz}$

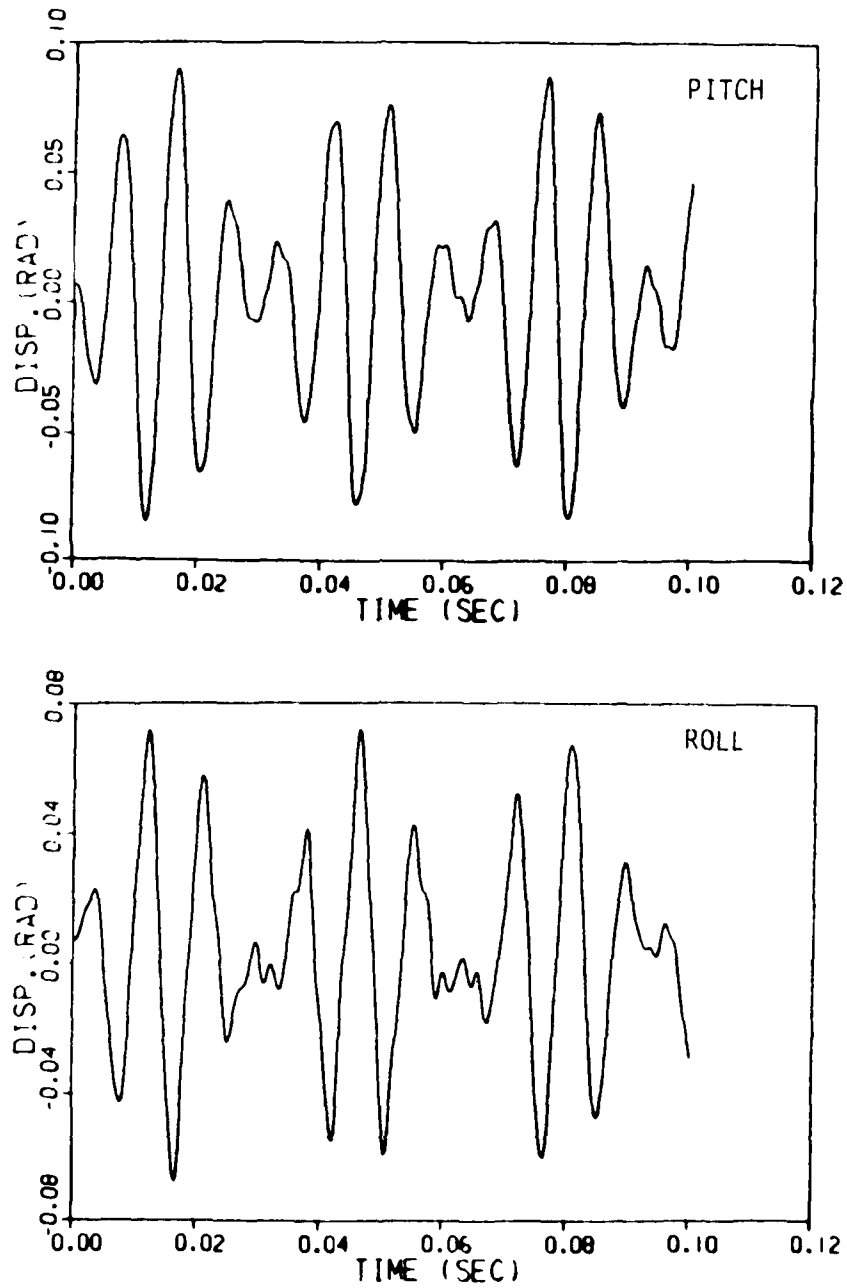


FIGURE 14 AERODYNAMIC SURFACE RESPONSE FOR A DYNAMIC PRESSURE OF 70 PSI

- o FLEXIBLE AERODYNAMIC SURFACE
- o TWO PRELOAD NONLINEARITIES
  - $S_\phi = S_\theta = 0.2 \text{ deg}$
  - $P_\phi = P_\theta = 0.1 \text{ deg}$
- o UNCOUPLED FREQUENCIES
  - $\omega_\phi = 215 \text{ Hz}$
  - $\omega_\theta = 60 \text{ Hz}$

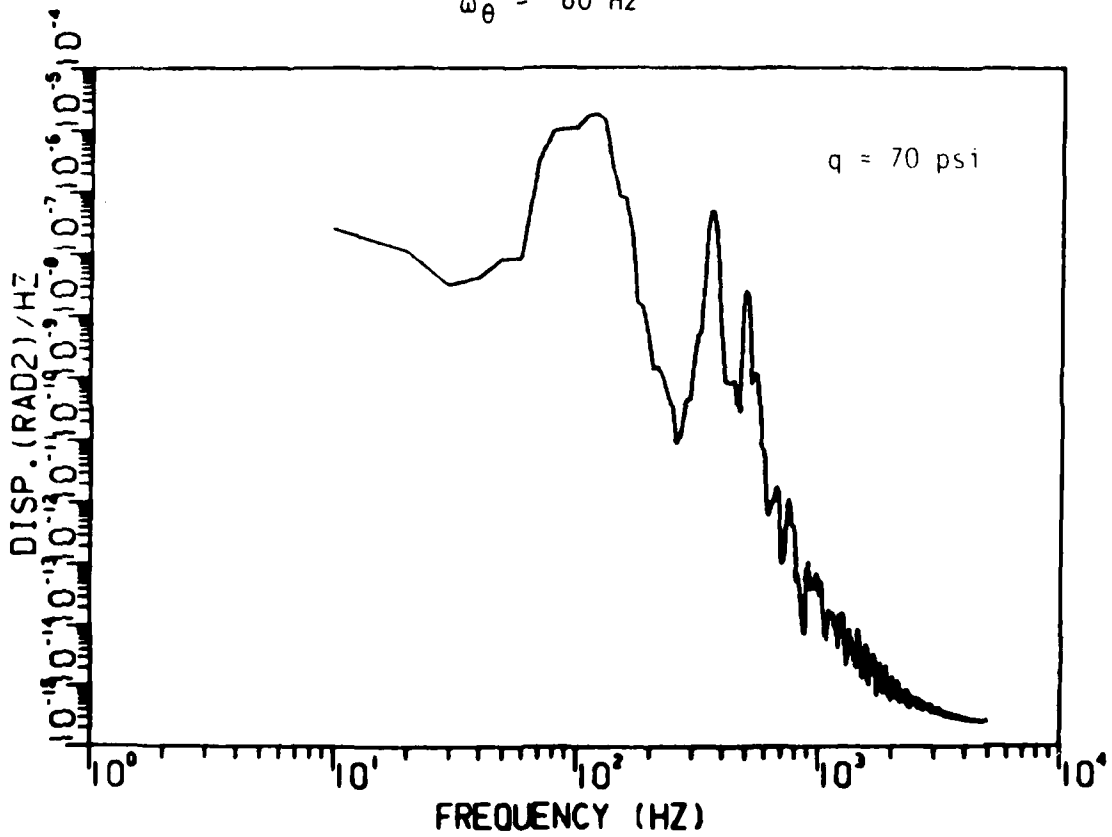


FIGURE 15 ROOT ROLL PSD FOR A DYNAMIC PRESSURE OF 70 PSI

this figure it appears that the lower two frequencies are merging toward a single value within the accuracy of the PSD plot. This is in fact the result which is indicated by the plot in Figure 13.

Referring to Figure 9, it is noted that the comparison between the three numerical simulation techniques and the approximate solution is inconclusive in the dynamic pressure range of 55 to 65 psi. In fact, the numerical results indicate a constant amplitude ratio, or "flat spot", over this range of dynamic pressures. This region of dynamic pressures precedes the changing of the response characteristics to that of a beat phenomenon. The implication of this response characteristic is discussed in Section 4.0.

#### 4.0 CONCLUSIONS

The objective of this study was to evaluate, on a comparative basis, several different type numerical simulation techniques for predicting the limit cycle response of an aerodynamic surface with structural nonlinearities. This objective was of interest since earlier studies, Reference 9, uncovered shortcomings with a "simple" trapezoidal integration scheme. Numerical data obtained with this trapezoidal approach were used for comparison with and evaluation of approximate solutions to the nonlinear problem. Based on these previous results, it was felt that the application of more refined integration techniques for nonlinear aerodynamic surfaces needed to be evaluated. Thus the present study was undertaken.

The objective of this study has been met. Limit cycle response predictions were obtained for the aerodynamic surface including discrete structural nonlinearities shown in Figure 1. These predictions were made employing the following three, quite different numerical integration schemes:

- Runge-Kutta
- Shanks
- Adams-Moulton

The results of the three simulation techniques compared well with each other. Thus it is concluded that any one of the numerical techniques is appropriate for the class of nonlinear problems associated with predicting limit cycle response of aerodynamic surfaces containing discrete structural nonlinearities. A second conclusion of this study is that the more refined numerical simulations yielded improved correlation with the approximate solution of Reference 9, when compared with the trapezoidal integration scheme.

Based on computational efficiency, the Runge-Kutta integration approach appears most attractive for these type problems. The normalized cost of the three techniques (CPU time, connect time, etc.) are shown in Figure 16. As can be seen, the Runge-Kutta approach is the most efficient technique. The Shanks technique is higher order than the Runge-Kutta method and requires significantly more calculations per time step. The Adams-Moulton procedure is a

Integration Technique	Cost Ratio
Runge-Kutta	1.0
Shanks	2.7
Adams-Moulton	5.0

FIGURE 16 COMPARISON OF COMPUTATIONAL EFFICIENCY FOR NUMERICAL INTEGRATION TECHNIQUES

predictor-corrector scheme and spends a great deal of time "stopping and starting."

In spite of the improved correlation obtained with the refined integration schemes, there remained regions where comparisons between the numerical simulation results and the approximate solutions were inconsistent. These inconsistencies were most apparent for a flexible aerodynamic control surface containing two root spring preload nonlinearities. Additionally, these inconsistencies appeared in limited regions of the nonlinear system response. This latter point is illustrated by the data presented in Figure 17. The trend in simulation results does not agree with the second order approximate solution in the region of dynamic pressure between 55 and 65 psi. As discussed in earlier paragraphs, limited analysis of the simulation results indicate that there appears to be a change in the nature of the limit cycle response in this region.

The mechanism of the nonlinear system response described in the preceding paragraph is not thoroughly understood. This indicates the need for additional research to provide an understanding of this nonlinear response phenomenon. Study activities are needed to provide explanations for the prediction inconsistencies noted in this study. Additional numerical simulations should be performed for regions deemed of interest, such as the "flat spot" noted in Figure 17. The influence of various parameters on the interpretation of these simulation results need to be evaluated. Significance of parameters such as simulation run time, initial condition magnitude and combination, and RMS amplitude determination need additional evaluation. In addition, detailed analyses of the frequency content of the numerically predicted system response are of interest. These activities will develop an improved understanding of the nonlinear response characteristics of an aerodynamic surface containing discrete structural nonlinearities.

- o FLEXIBLE AERODYNAMIC SURFACE
- o TWO PRELOAD NONLINEARITIES
  - $S_\phi = S_\theta = 0.2 \text{ deg}$
  - $P_\phi = P_\theta = 0.1 \text{ deg}$
- o UNCOUPLED FREQUENCIES
  - $\omega_\phi = 215 \text{ Hz}$
  - $\omega_\theta = 60 \text{ Hz}$

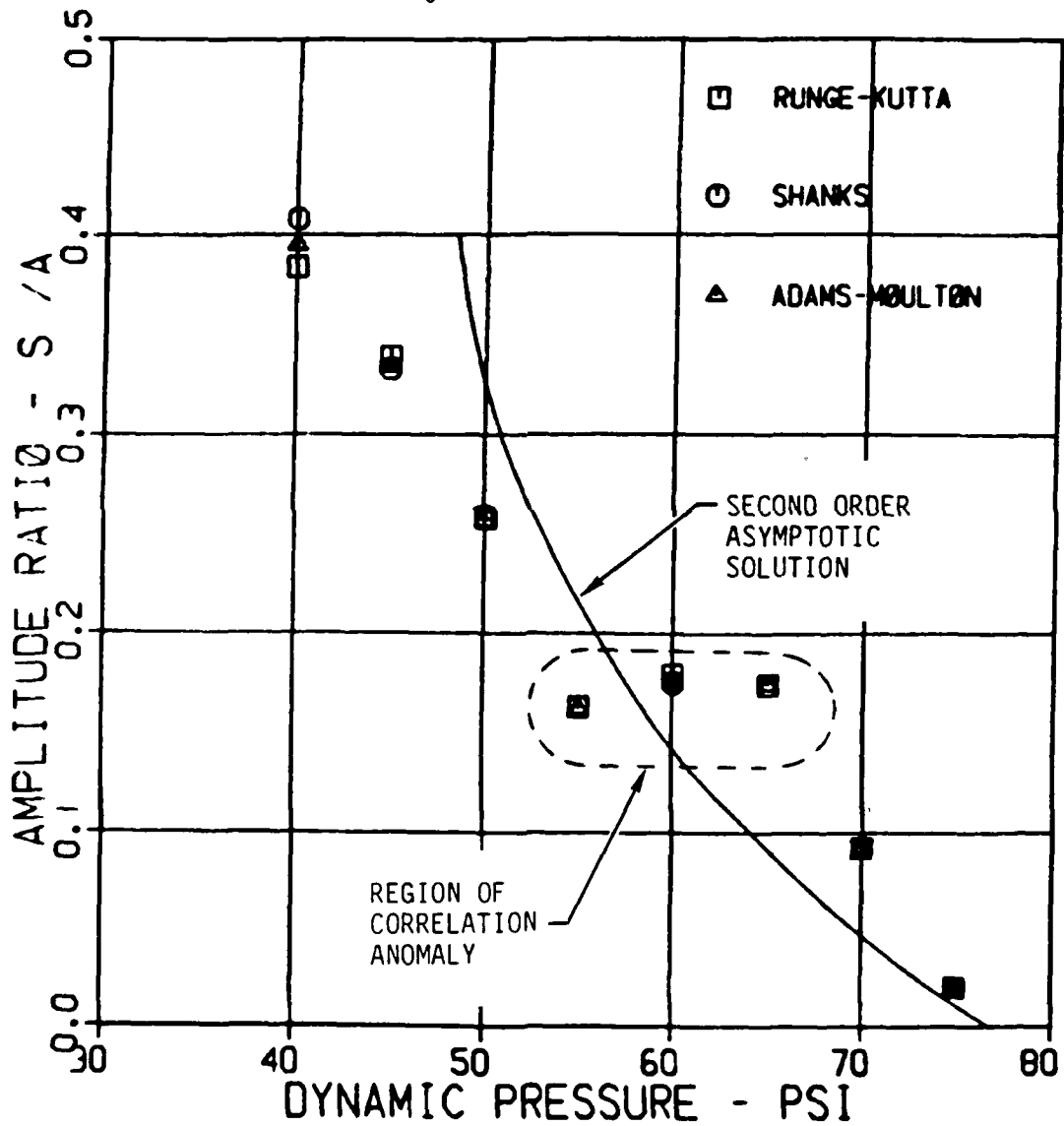


FIGURE 17 REGION OF CORRELATION ANOMALY

## 5.0 REFERENCES

1. Woolston, D.S., Runyan, H.L., and Andrews, R.E., "An Investigation of Effects of Certain Types of Structural Nonlinearities on Wing and Control Surface Flutter," *Journal of the Aeronautical Sciences*, Vol. 24, January 1957, pp. 57-63.
2. Shen, S.F., "An Approximate Analysis of Nonlinear Flutter Problems," *Journal of the Aerospace Sciences*, Vol. 26, January 1959, pp. 25-32, 45.
3. Breitback, E., "Effects of Structural Non-Linearities on Aircraft Vibration and Flutter," AGARD-R-655, January 1978.
4. Laurenson, R.M., and Trn, R.M., "Flutter of Control Surfaces with Structural Nonlinearities," *AIAA Journal*, Vol. 18, No. 10, October 1979, pp. 1245-1251.
5. Breitback Elmar J., "Flutter Analysis of a Airplane With Multiple Structural Nonlinearities in the Control System," NASA TP-1620, March 1980.
6. Briley, R.P. and Laurenson, R.M., "Flutter of Control Surfaces with Structural Nonlinearities, Phase II," Report MDC E2352, McDonnell Douglas Astronautics Company - St. Louis Division, Final Report (Contract N00019-76-C-606), May 1980.
7. Desmarais, R.N. and Reed, W.H., "Wing Store Flutter with Nonlinear Pylon Stiffness," AIAA/ASME/ASCE/AHS Structures, Structural Dynamics and Material Conference, Seattle, WA, 12-14 May 1980, AIAA Paper 80-0792.
8. McIntosh, S.C., Reed, R.E., Jr., and Rodeen, W.P., "Experimental and Theoretical Study of Nonlinear Flutter," *Journal of Aircraft*, Vol. 18, No. 12, December 1981, pp. 1057-1063.

9. Briley, R.P. and Gubser, J.L., "Investigation of Limit Cycle Response of Aerodynamic Surfaces With Structural Nonlinearities," McDonnell Douglas Astronautics Company-St. Louis, Final Report (Contract F49620-82-C-0043), November 1982.
10. Dahlquist, Germund, and Björck, Åke, Numerical Methods, Prentice-Hall, Inc., Englewood Cliffs, NJ, 1974, translated by Ned Anderson, pp. 347.
11. Boyce, W.E. and Diprima, R.C., Elementary Differential Equations and Boundary Value Problems, John Wiley & Sons, Inc., New York, NY, 3rd ed., 1977, Chap. 8.
12. Shanks, E.B., "Higher Order Approximations of Runge-Kutta Type," NASA TN-D2920, September 1965.
13. CYBER Service Library Reference Manual, McDonnell Douglas Automation Company, McAuto Publication M4945011, April 1984, pp III-2-36 through III-2-50.

APPENDIX A  
AERODYNAMIC SURFACE CONFIGURATION

Properties of the Harpoon missile quick-attach control surface were used to define the aerodynamic surface configuration used throughout this study. The geometric configuration of the aerodynamic surface is shown in Figure A1. The structural nonlinearities that were investigated are associated with root support structure. Presented in Figure A2 are the inertia properties of the aerodynamic surface. These are the specific terms of the inertia matrix of Equation (2). The first two rows and columns of the inertia matrix are associated with rigid root roll and pitch motions while the last two diagonal elements are the generalized masses of the aerodynamic surface modes. The off-diagonal terms, the PF quantities, represent the inertia coupling between rigid and flexible motions. The mode shapes associated with the first two aerodynamic surface cantilever modes are given in Figure A3. These modal data were used when investigating a flexible surface configuration.

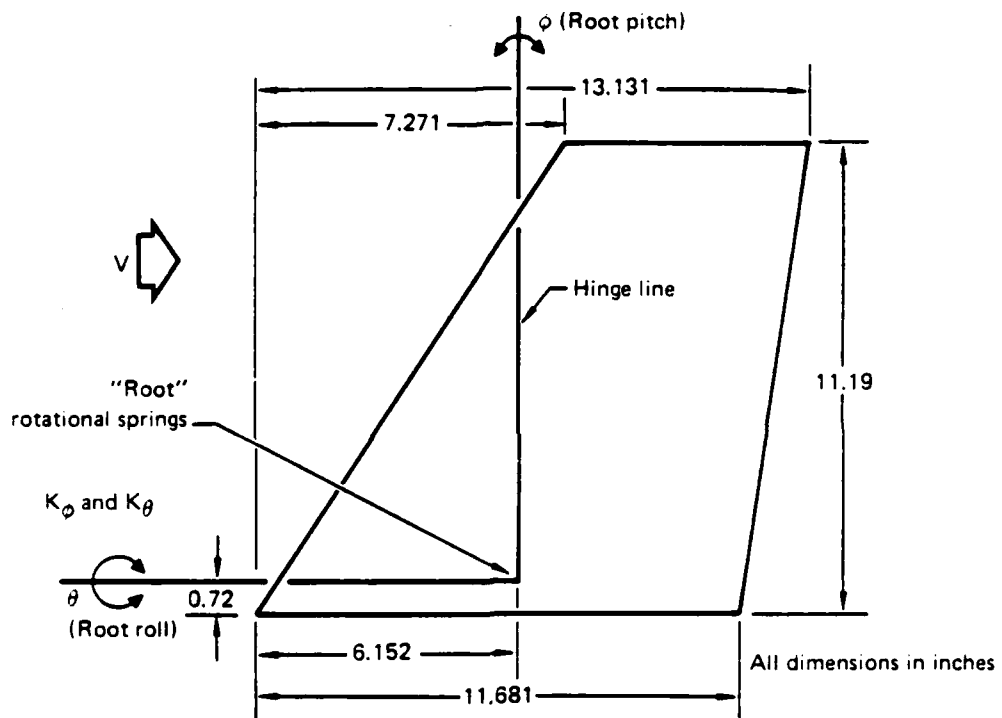


FIGURE A1 AERODYNAMIC SURFACE GEOMETRY

$$\begin{bmatrix} I_{\theta} & I_{\theta\phi} & PF_{\theta 1} & PF_{\theta 2} \\ & I_{\phi} & PF_{\phi 1} & PF_{\phi 2} \\ & & m_1 & 0 \\ \text{Symmetric} & & & m_2 \end{bmatrix}$$

(a) Form of Inertia matrix

$I_{\theta} = 0.1667 \text{ lb-sec}^2\text{-in.}$	$PF_{\theta 1} = -7.227 \times 10^{-3} \text{ lb-sec}^2$
$I_{\phi} = 0.071 \text{ lb-sec}^2\text{-in.}$	$PF_{\theta 2} = -1.014 \times 10^{-3} \text{ lb-sec}^2$
$I_{\theta\phi} = 0.058 \text{ lb-sec}^2\text{-in.}$	$PF_{\phi 1} = -3.212 \times 10^{-3} \text{ lb-sec}^2$
$m_1 = 4.220 \times 10^{-4} \text{ lb-sec}^2/\text{in.}$	$PF_{\phi 2} = 2.134 \times 10^{-3} \text{ lb-sec}^2$
$m_2 = 4.295 \times 10^{-4} \text{ lb-sec}^2/\text{in.}$	

(b) Specific inertia terms

FIGURE A2 AERODYNAMIC SURFACE INERTIA PROPERTIES

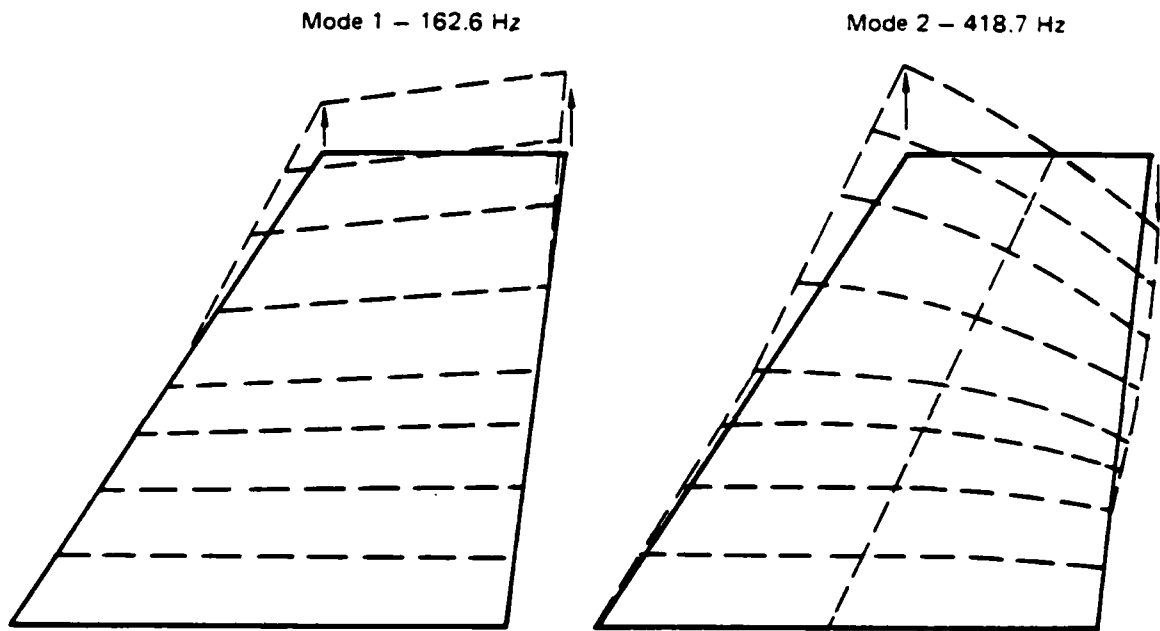


FIGURE A3 AERODYNAMIC SURFACE CANTILEVER MODES

APPENDIX B  
SIMULATION RESULTS FOR FLEXIBLE AERODYNAMIC SURFACE

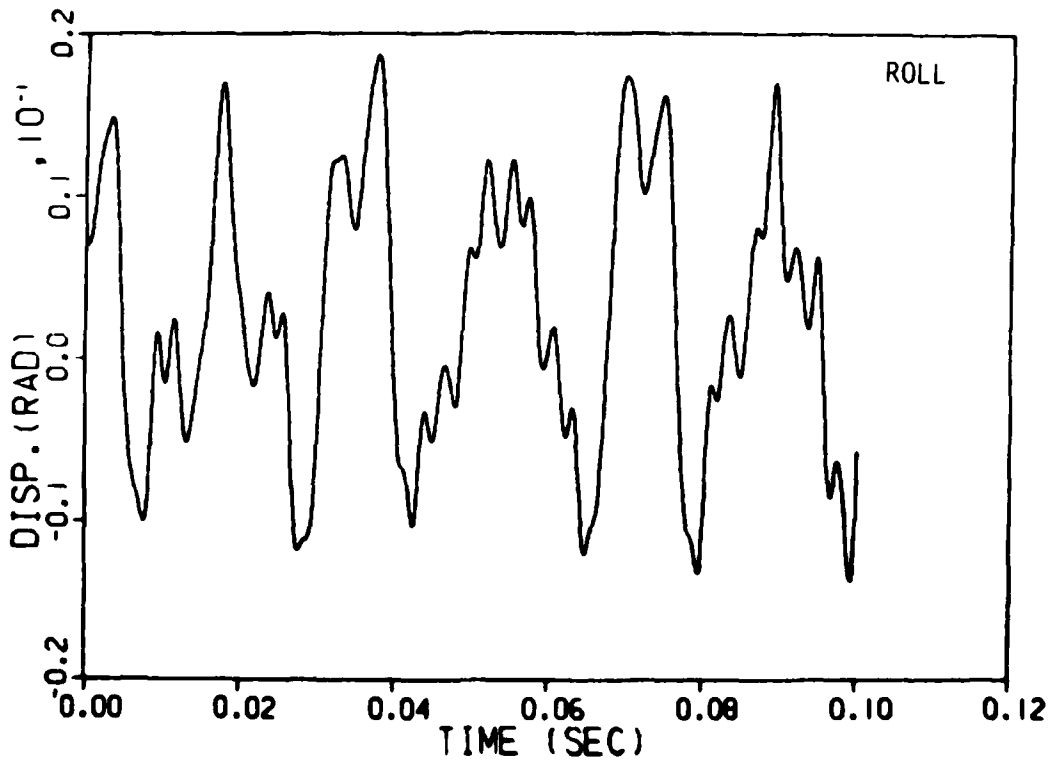
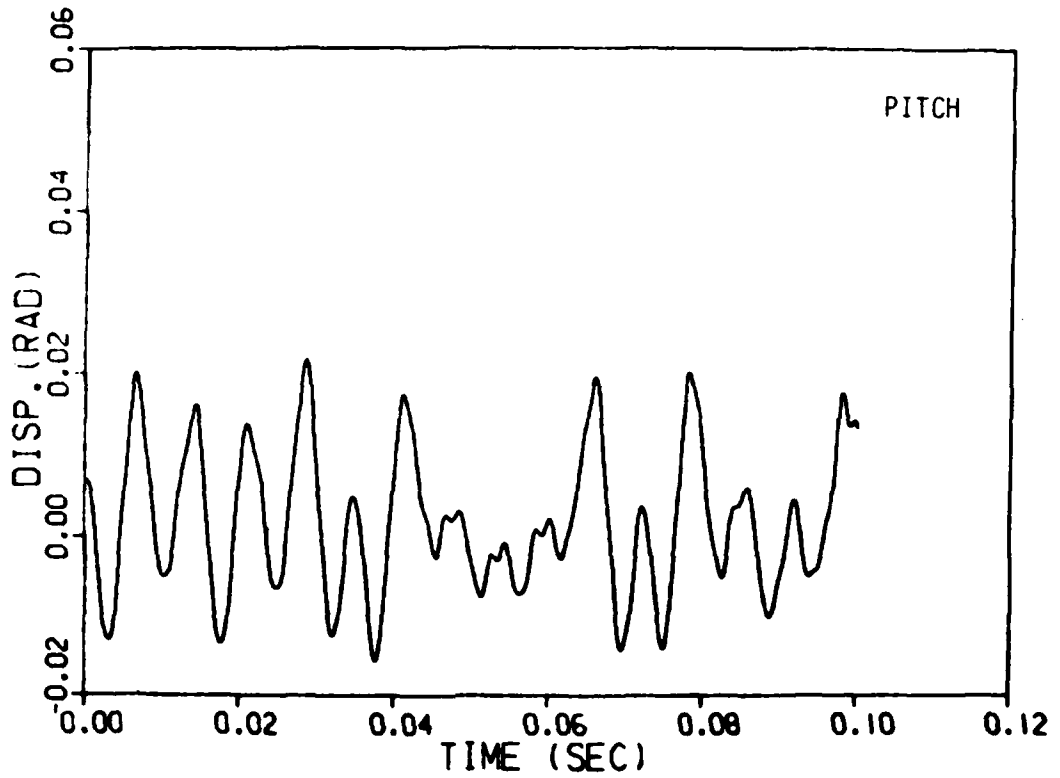
Presented on the following pages are plots of the root roll and root pitch response obtained from the numerical simulation for the flexible aerodynamic surface. These results were obtained for a surface having two preload nonlinearities with the following characteristics:

$$S_{\phi} = S_{\theta} = 0.2 \text{ deg}$$

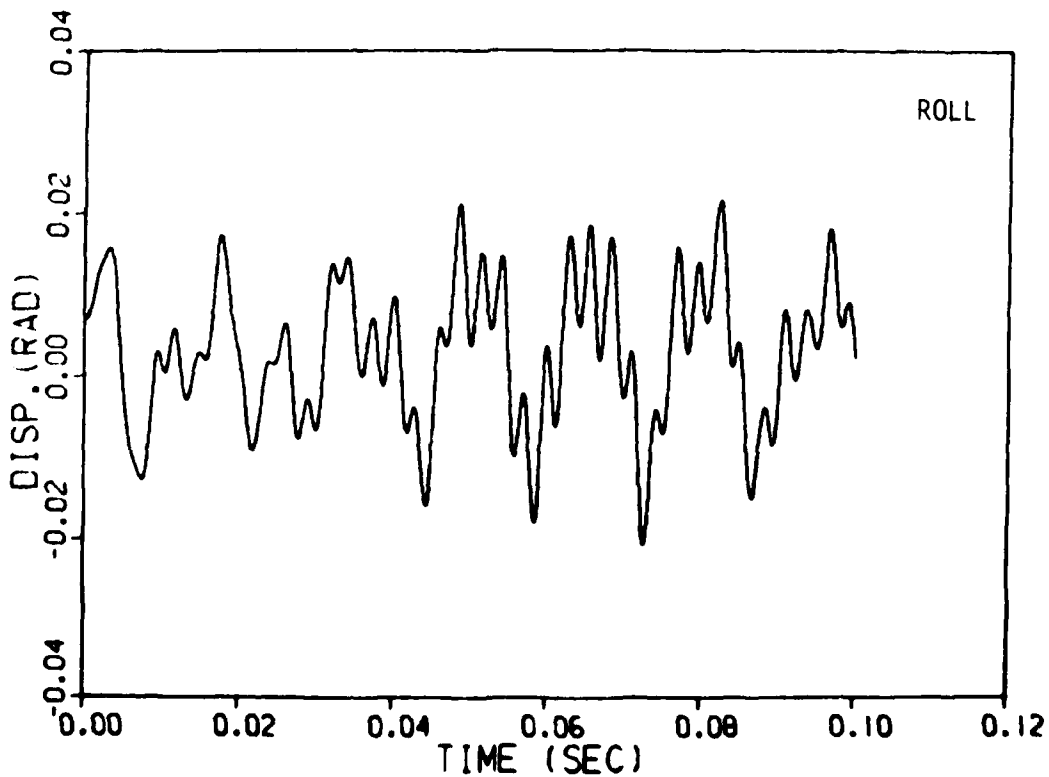
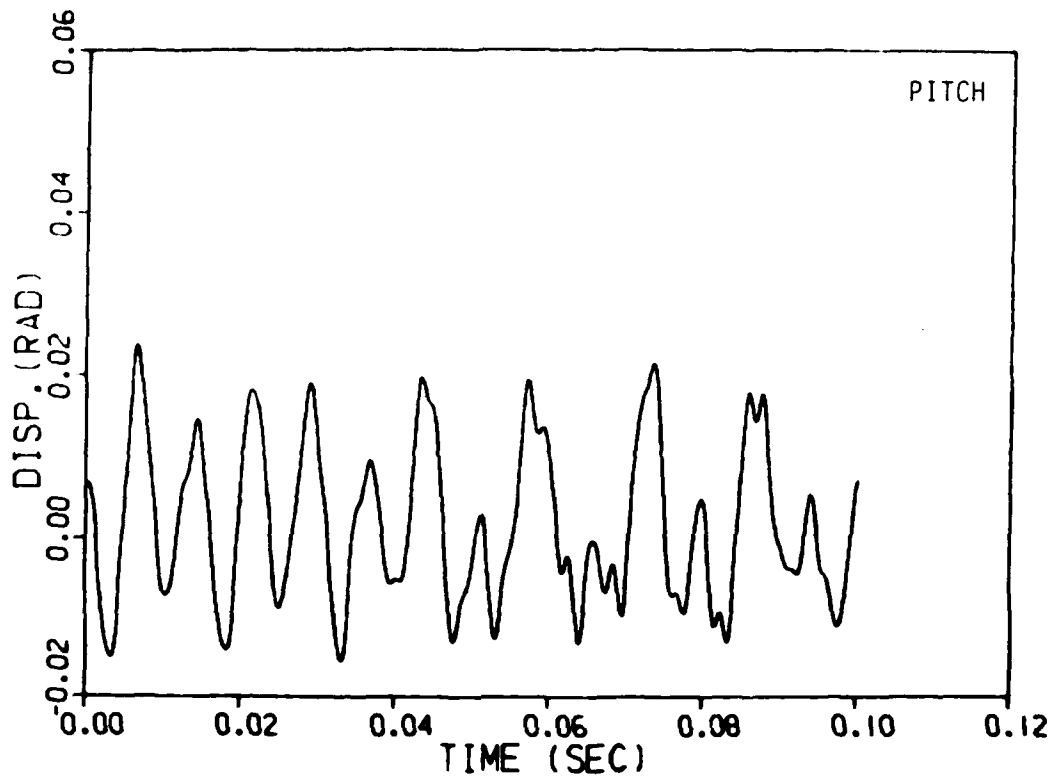
$$P_{\phi} = P_{\theta} = 0.1 \text{ deg}$$

In addition, the uncoupled root roll frequency ( $\omega_{\theta}$ ) was 60 Hz and the pitch frequency ( $\omega_{\phi}$ ) was 215 Hz for these simulation cases. The plots on the following pages formed the basis for obtaining the results presented in Figures 12 and 13.

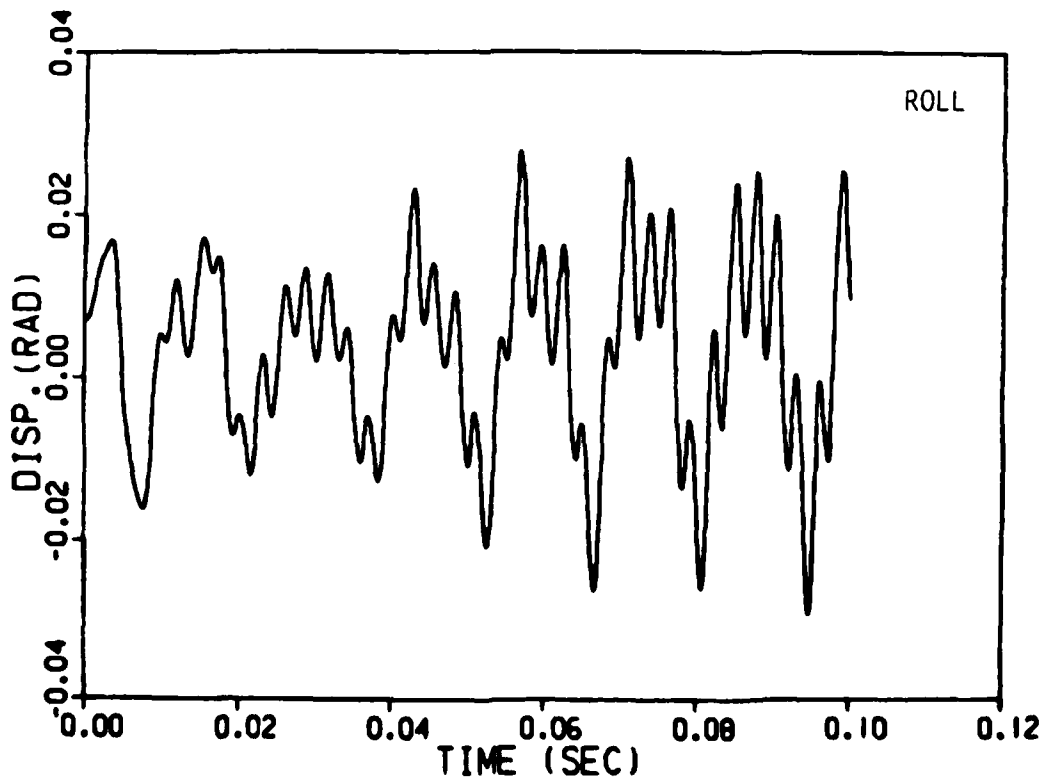
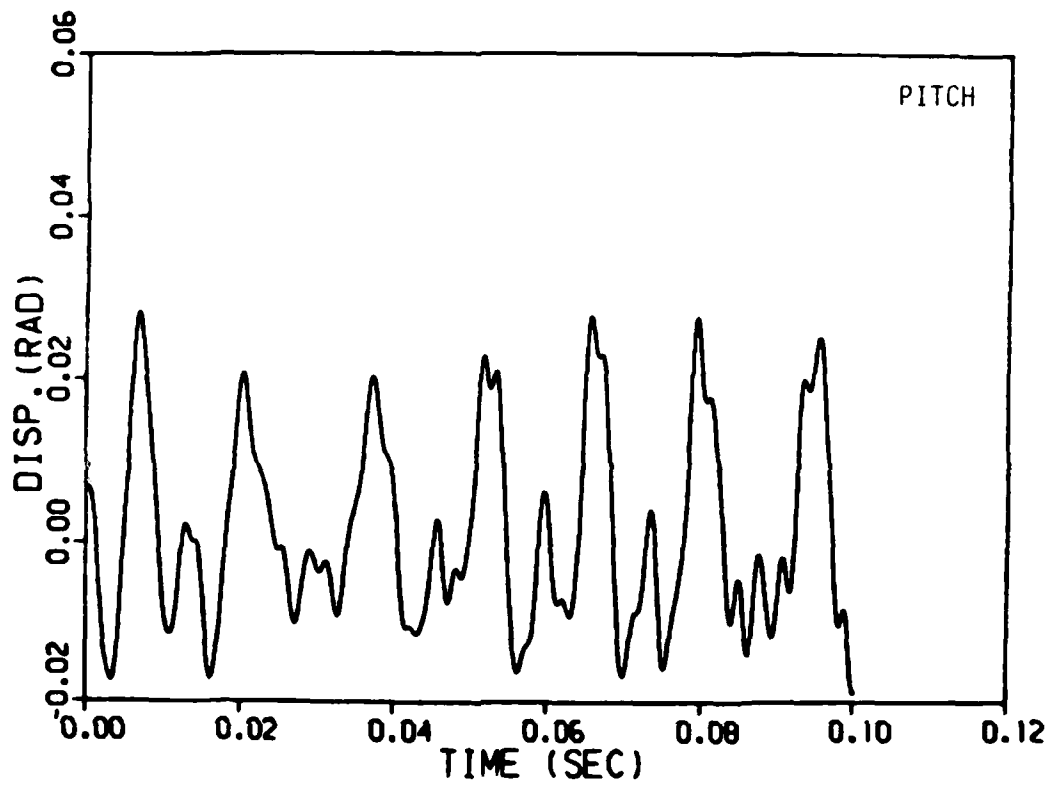
DYNAMIC PRESSURE OF 40 PSI



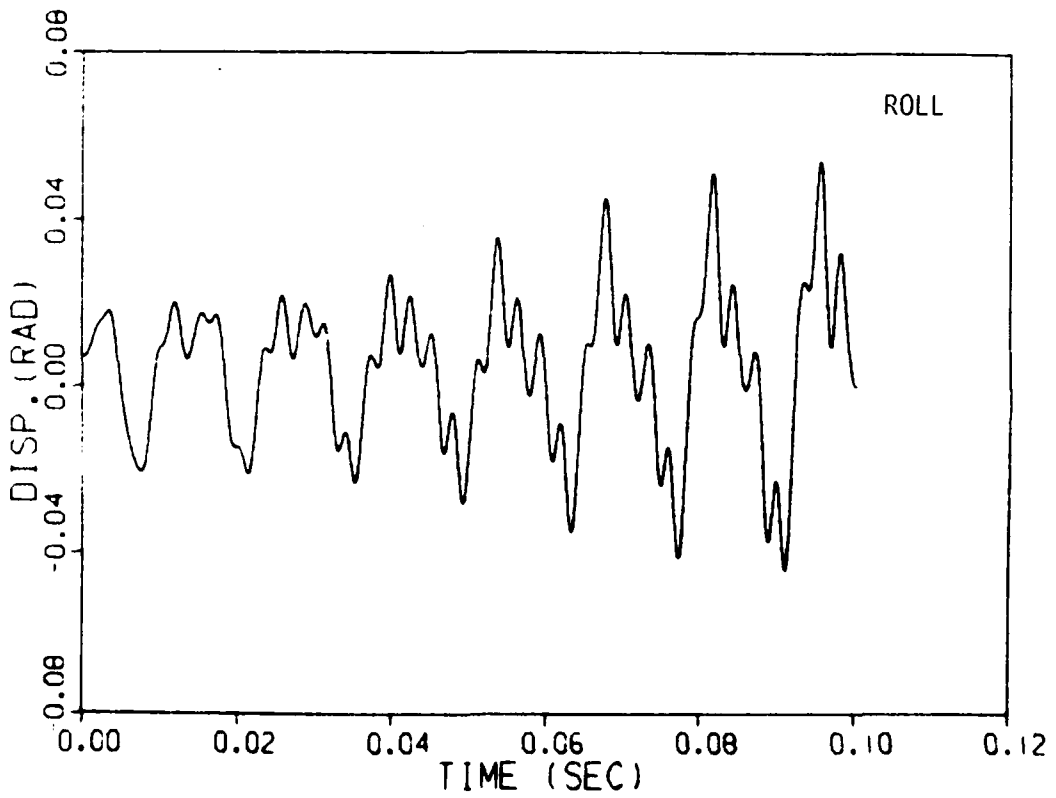
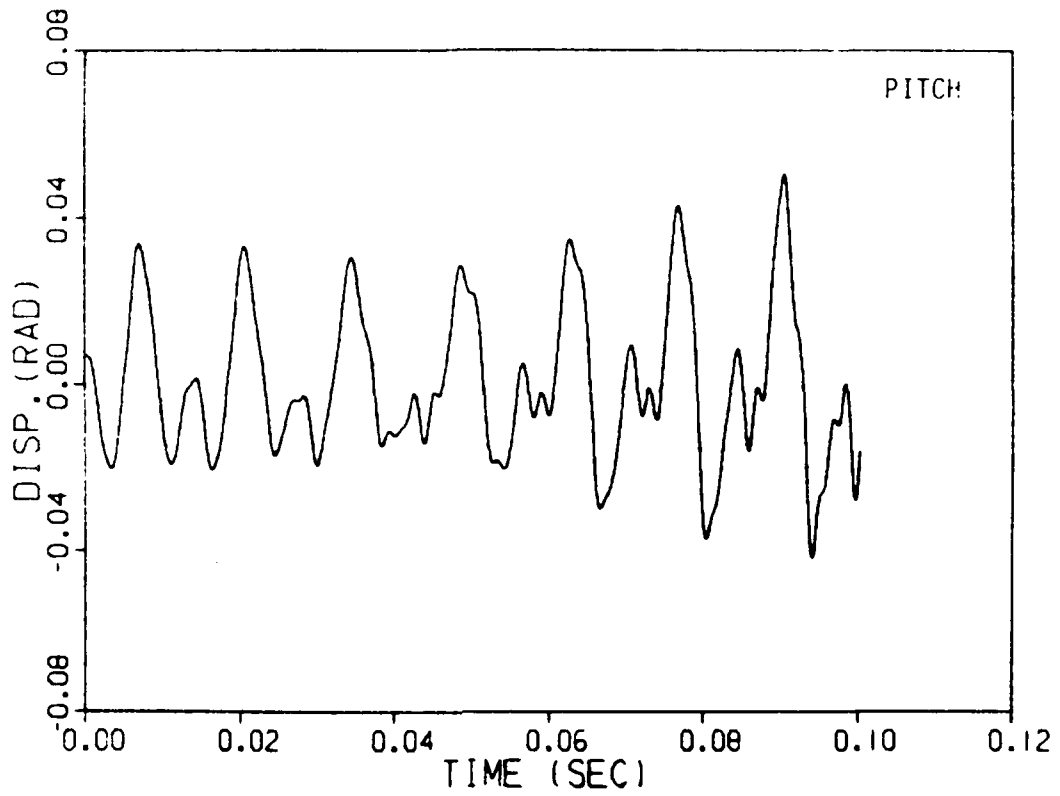
DYNAMIC PRESSURE OF 45 PSI



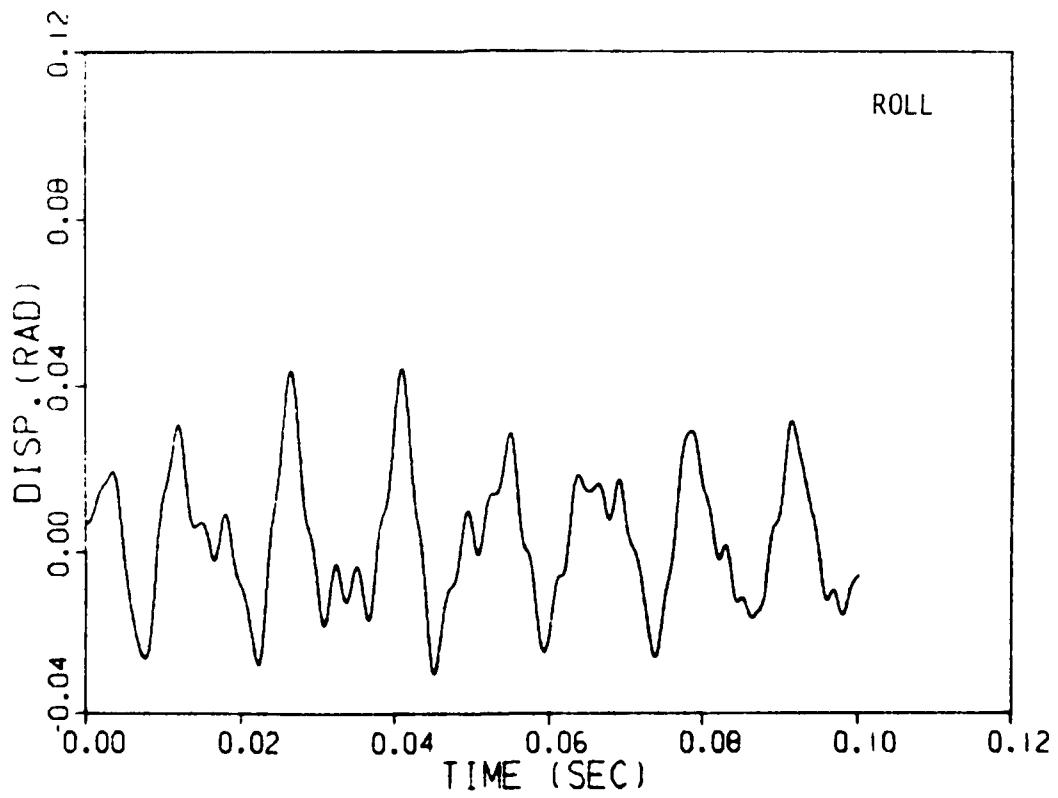
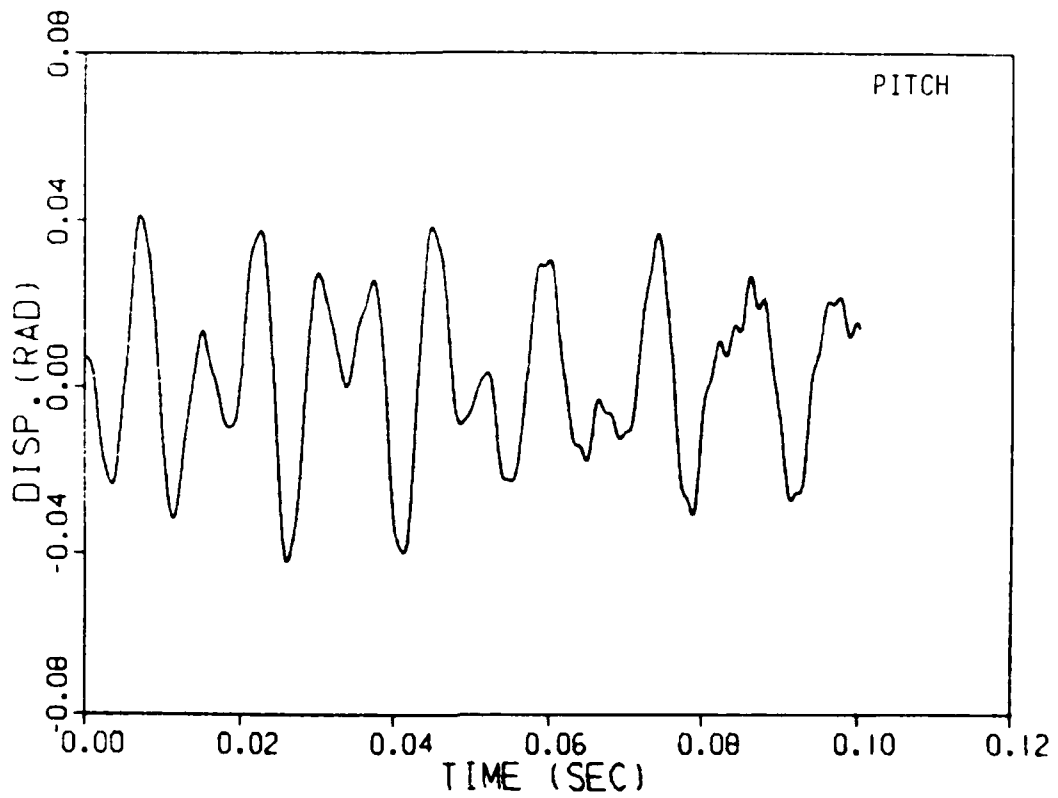
DYNAMIC PRESSURE OF 50 PSI



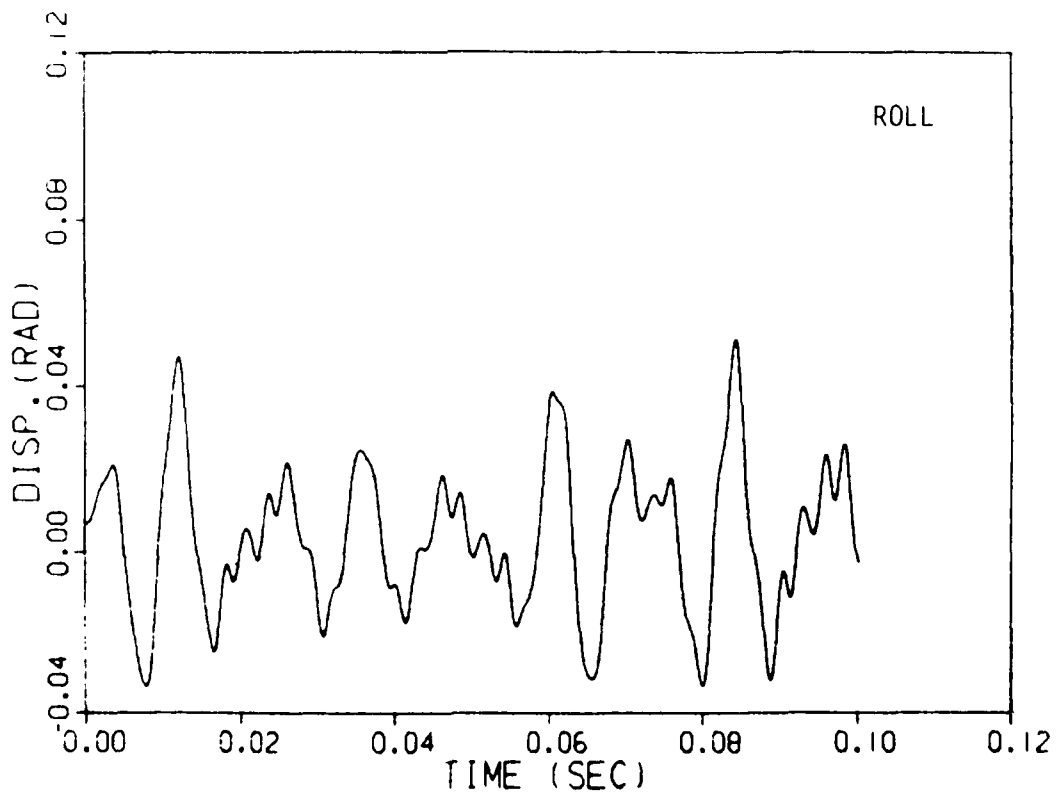
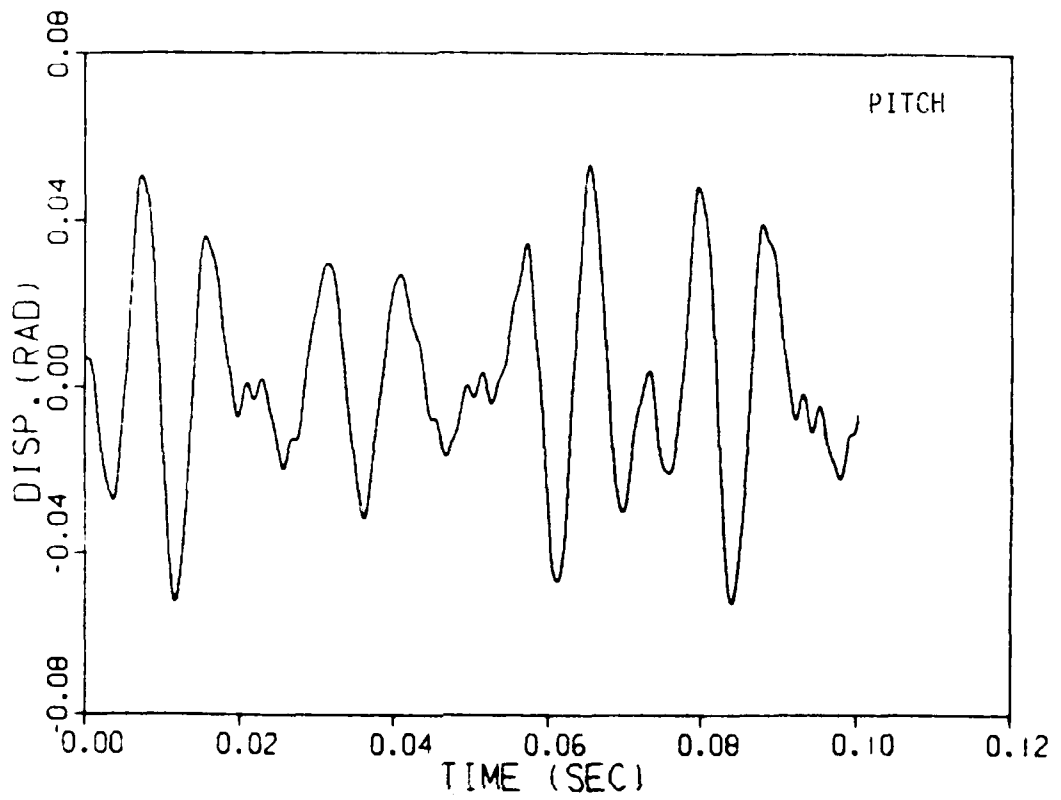
DYNAMIC PRESSURE OF 55 PSI



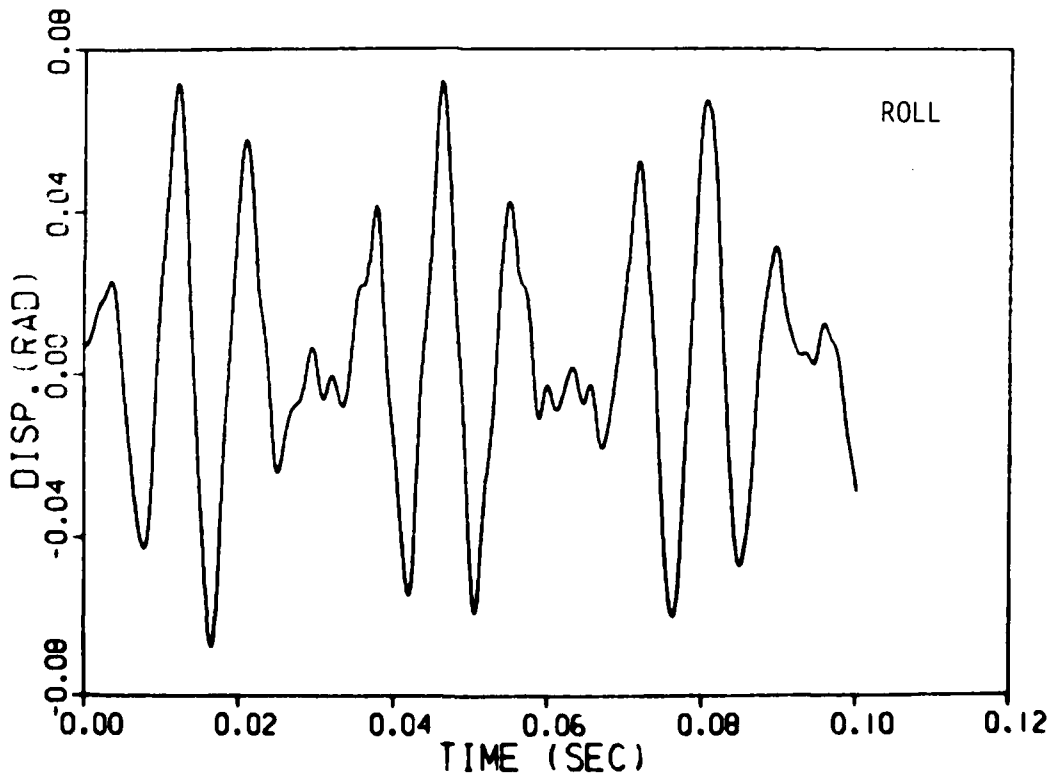
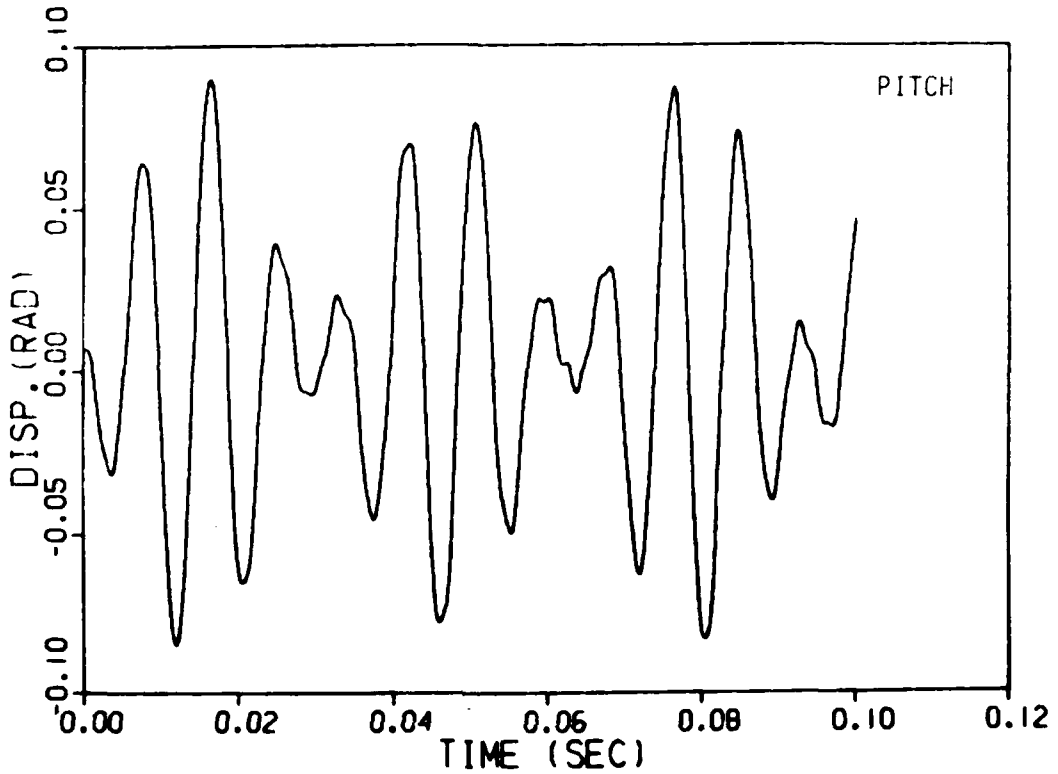
DYNAMIC PRESSURE OF 60 PSI



DYNAMIC PRESSURE OF 65 PSI



DYNAMIC PRESSURE OF 70 PSI



DYNAMIC PRESSURE OF 75 PSI

